IAEA nuclear fusion

SPECIAL TOPIC • OPEN ACCESS

Spherical tokamak physics research in preparation for the operation of NSTX-U

To cite this article: S. Munaretto *et al* 2026 *Nucl. Fusion* **66** 035001

IOP Publishing | International Atomic Energy Agency
Nuclear Fusion
Nucl. Fusion **66** (2026) 035001 (20pp)
https://doi.org/10.1088/1741-4326/ae38f6

Special Topic

Spherical tokamak physics research in preparation for the operation of NSTX-U

S. Munaretto[1,*], P.O. Adebayo-Ige[2], H. Anand[3], G. Avdeeva[3], S.G. Baek[4], K. Barada[5], E. Belli[3], E.V. Belova[1], J.W. Berkery[1], T.N. Bernard[3], N. Bertelli[1], P. Bonofiglo[1], P.T. Bonoli[4], M.D. Boyer[6], J. Candy[3], C.S. Chang[1], H. Chung[7], C. Clauser[4], M. Comanescu[1], D. Corona[1], N.A. Crocker[5], R. De Levante Rodriguez[4], E.W. DeShazer[3], A. Diallo[1], J. Dominski[1], V.N. Duarte[1], F. Ebrahimi[1], E.D. Emdee[1], S. Ethier[1], N.M. Ferraro[1], E.L. Foley[8], E.D. Fredrickson[1], M.E. Galante[8], K.F. Gan[2], S. Gerhardt[1], R.J. Goldston[1], M. Gorelenkova[1], W. Guttenfelder[9], R. Hager[1], F.D. Halpern[3], J. Halpern[10], D. Hatch[11], F. Hoffmann[1], M.S. Islam[12], S.C. Jardin[1], S.M. Kaye[1], A. Khodak[1], J.E. Kinsey[13], A. Kleiner[1], E. Kolemen[14], S. Ku[1], M. Lampert[1], B. Leard[15], B.P. LeBlanc[1], J.B. Lestz[3], F.M. Levinton[8], P.-Y. Li[11], N.C. Logan[10], N.A. Lopez[16], R. Lunsford[1], T. Macwan[5], R. Maingi[1], J. McClenaghan[3], A.G. McLean[12], J.E. Menard[1], Y.-S. Na[7], A.O. Nelson[10], M. Ono[1], A. Pajares[3], A. Pankin[1], J. Parisi[17], F.I. Parra[1], M.S. Parsons[1], B.S. Patel[18], M. Podestá[19], F.M. Poli[20], M. Porcelli[1], T. Rafiq[15], R. Raman[21], J.D. Riquezes[10], S.A. Sabbagh[10], A. Sanchez-Villar[1], E. Schuster[15], S. Shiraiwa[1], T. Singh[15], S.P. Smith[3], D. Smith[22], V.A. Soukhanovskii[12], G.M. Staebler[23], B. Stratton[1], K.E. Thome[3], M. Tobin[10], I.U. Uzun-Kaymak[8], B. Van Compernolle[3], W.X. Wang[1], W. Wehner[3], A.S. Welander[3], B.D. Wirth[2], J. Yang[1], V. Zamkovska[10] and X. Zhang[16]

[1] Princeton Plasma Physics Laboratory Princeton, NJ, United States of America
[2] University of Tennessee, Knoxville, TN, United States of America
[3] General Atomics, San Diego, CA, United States of America
[4] Massachusetts Institute of Technology, Cambridge, MA, United States of America
[5] University of California at Los Angeles, Los Angeles, CA, United States of America
[6] Commonwealth Fusion Systems, Devens, MA, United States of America
[7] Seoul National University, Seoul, Korea, Republic Of
[8] Nova Photonics, Princeton, NJ, United States of America
[9] Type One Energy, Madison, WI, United States of America
[10] Columbia University, NY, NY, United States of America
[11] The University of Texas at Austin, Austin, TX, United States of America
[12] Lawrence Livermore National Laboratory, Livermore, CA, United States of America
[13] CompX, Del Mar, CA, United States of America
[14] Princeton University, Princeton, NJ, United States of America

[*] Author to whom any correspondence should be addressed.

[15] Lehigh University, Bethlehem, PA, United States of America
[16] Tokamak Energy Ltd., Milton Park, United Kingdom of Great Britain and Northern Ireland
[17] Marathon Fusion, San Francisco, CA, United States of America
[18] United Kingdom Atomic Energy Authority, Abingdon, United Kingdom of Great Britain and Northern Ireland
[19] Ecole Polytechnique Fédérale de Lausanne, Swiss Plasma Center, Lausanne, Switzerland
[20] ITER Organization, St. Paul Lez Durance, France
[21] University of Washington, Seattle, WA, United States of America
[22] University of Wisconsin, Madison, WI, United States of America
[23] Oak Ridge National Laboratory, Oak Ridge, TN, United States of America

E-mail: smunaret@pppl.gov

Received 6 November 2025, revised 9 December 2025
Accepted for publication 15 January 2026
Published 2 February 2026

Abstract

The National Spherical Torus Experiment Upgrade (NSTX-U) is preparing to resume operation, representing a crucial step toward realizing compact, cost-effective fusion pilot plants. In advance of this, extensive modeling and data analysis have been conducted to advance the physics basis for low-aspect-ratio, high-performance plasma regimes, focusing on three core objectives: confinement and stability, power and particle handling, and steady-state operation. Significant progress has been made in understanding the electron temperature flattening in high-β plasmas, which is shown to be driven by a complex interplay of magnetohydrodynamic instabilities (e.g. non-resonant infernal modes), fast-ion-driven Alfvén eigenmodes, and electron and ion-scale micro-instabilities, particularly Kinetic Ballooning Modes (KBMs), whose destabilization is strongly dependent on parallel magnetic field fluctuations ($\delta B_{\|}$). Furthermore, a new gyrokinetic critical pedestal model was developed, accurately predicting pedestal structure by identifying KBMs as the primary stability limit, offering a critical constraint for future high-confinement scenarios. To address the challenge of high heat flux, novel liquid lithium plasma-facing components were modeled. The analysis confirmed that lithium vapor shielding is a self-regulating mechanism for heat mitigation, while also emphasizing that strong main ion parallel flow is essential to minimize core lithium contamination. Finally, progress toward steady-state operation was anchored by developing the required physics basis and control tools. This includes predictive modeling for reversed magnetic shear sustainment, demonstrating that magnetic island-induced bootstrap current reduction is negligible in STs, and advancing real-time control and disruption avoidance capabilities. The development of high-speed surrogate models (e.g. MMMNet) provides computationally efficient tools vital for non-inductive scenario optimization and integrated, low-disruptivity operations planned for NSTX-U.

Keywords: NSTX-U, spherical Tokamak, overview

(Some figures may appear in colour only in the online journal)

1. Introduction

Spherical Tokamaks (STs) represent a potentially transformative path toward more compact and cost-effective Fusion Pilot Plants (FPPs) [1–3], a design actively being explored by both public and private entities [4–6]. After a period of repair, the National Spherical Torus Experiment Upgrade (NSTX-U) [7] at the Princeton Plasma Physics Laboratory is preparing to resume operations in 2026. In the interim, and in conjunction to collaborating with other international STs [8–12], ongoing data analysis and modeling continue to advance the physics basis needed for these next-generation devices.

The primary appeal of the ST configuration is its potential for high performance in a smaller device. Its low aspect ratio (A), and therefore its relatively lower toroidal magnetic field (B_T), allows for high β (the ratio of plasma pressure to magnetic pressure), which is key to enabling more economical power generation. The upgraded NSTX-U facility is uniquely equipped to explore these potentialities with its significantly expanded capabilities, including a planned 2 MA of plasma current, a 1 T toroidal field, and a combined 18 MW of auxilary heating power. These enhancements will allow NSTX-U to operate at much lower plasma collisionality than its predecessor NSTX [13], a key parameter where STs are predicted to have a strong confinement advantage over conventional tokamaks [14]. Furthermore, NSTX-U provides an invaluable environment for studying critical physics relevant to burning plasmas since its energetic beam ions mimic the behavior of alpha particles expected in FPPs.

The compact design of STs also presents a critical challenge, however: managing the extreme heat fluxes on plasma-facing components (PFCs). NSTX-U is uniquely positioned also to address this problem. It is designed to operate in regimes that produce unmitigated peak heat fluxes of up to $100\,\mathrm{MW\,m^{-2}}$, making it an ideal testbed for developing and validating innovative solutions to reduce these intense heat loads to manageable levels.

To bridge the gap between current experiments and future FPPs, the NSTX-U research mission is centered on three main objectives:

- Extend confinement and stability physics basis at low-A and high beta to lower collisionality relevant to burning plasma regimes;
- Develop and evaluate conventional and innovative power and particle handling techniques to optimize plasma exhaust in high performance scenarios;
- Develop core-edge integrated operation at large bootstrap fraction and advance the physics basis required for non-inductive, high-performance and low-disruptivity operation of steady-state compact fusion devices.

The paper summarizes the work done since the publication of [15] to achieve these objectives. It is organized in three main sections, each addressing one of them, in the same order as listed above.

2. Extending high-beta, low-*A* confinement & stability physics to low collisionality

The primary goal of this objective is to advance the physics basis required to understand, predict, and optimize core plasma performance at low aspect ratio and reduced collisionality relevant to future fusion devices. The work toward this goal has recently been focused primarily on three areas, whose main achievements are summarized below.

2.1. Progress in understanding the flattening of the electron temperature radial profile

The observed flattening of the electron temperature (T_e) profiles in high-performance NSTX plasmas presents a significant impediment to sustaining these regimes and maximizing fusion output. This phenomenon, characterized by the central T_e remaining constant even with increasing heating power, indicates underlying mechanisms of enhanced core transport or compromised heating efficiency. Progress was made in order to comprehensively explain this observed T_e flattening with efforts that delved into distinct yet interconnected processes: magnetohydrodynamic (MHD) instabilities; fast-ion driven modes; and ion and electron-scale micro-instabilities.

2.1.1. Role of MHD instabilities. One critical avenue for understanding T_e flattening is the role of core MHD instabilities, particularly in plasmas with non-monotonic safety factor (q) profiles, also called reversed magnetic shear (RMS). It was shown through M3D-C1 [16] simulations that an MHD event in NSTX shot 129169, which terminated a RMS period, led to an abrupt lowering of the central safety factor (q_0) and a greatly reduced peakedness of the pressure profile [17, 18]. The analysis showed that as the minimum safety factor decreased, the dominant instability shifted from a double tearing mode toward a non-resonant pressure driven MHD mode known as infernal mode [19, 20]. Just before the experimentally observed MHD event, the equilibrium was found to be linearly unstable to several pressure-driven infernal modes, but a non-resonant pressure-driven ($n = 1$, $m = 1$) mode dominated the nonlinear evolution, where n and m are the toroidal and poloidal mode numbers. This (1,1) mode caused large changes in the central q and pressure values, resulting in a final state with a reduced and flattened pressure profile and a nearly monotonic q-profile, which aligns qualitatively with experimental observations. The flattening of the pressure profile directly implies a flattening of the temperature profile due to energy redistribution. Moreover, earlier studies on monotonic q-profile discharges revealed that such MHD instabilities could destroy innermost flux surfaces, leading directly to a flattening of the electron temperature profile by enhancing heat transport across the magnetic field [21–23]. Figure 1 shows the experimentally reconstructed q and surface-averaged pressure profiles over time, and the predicted ones by M3D-C1, clearly showing the reduction and flattening of the pressure profile. Studies presented in section 4.1 investigate possible paths to sustain the RMS configurations in future NSTX-U plasmas, and therefore avoid the flattening of the T_e profile observed in NSTX.

2.1.2. Role of fast-ion driven Alfvén eigenmodes. Global Alfvén Eigenmodes (GAEs) and Compressional Alfvén Eigenmodes (CAEs) are frequently observed during neutral beam injection (NBI) in NSTX/NSTX-U, and have been correlated with T_e profile flattening [24]. After investigating their nonlinear dynamics, it was observed that these modes can enhance electron transport through various mechanisms, including parallel electric fields, electron orbit stochasticity, or energy channeling [25]. Nonlinear simulations, encompassing both single-toroidal mode number and full nonlinear runs, revealed a significant redistribution of resonant fast ions, particularly in their pitch parameter. This redistribution primarily acts to reduce the anisotropy driving the instability and can

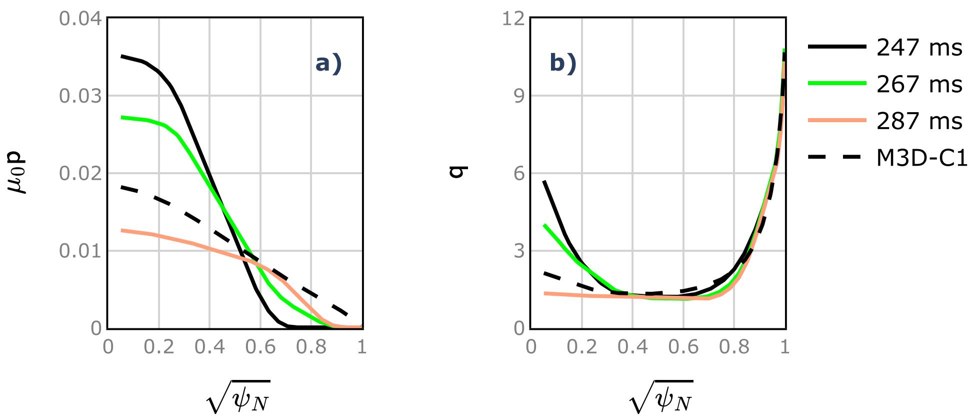

Figure 1. Surface averaged pressure profile (*a*) and q-profile (*b*). With solid lines the experimentally reconstructed profiles from NSTX shot 129169 at three different times. In dashed black lines the profiles at the end of the M3D-C1 3D nonlinear calculation, started from the profiles at $t = 247$ ms. Reproduced from [17]. CC BY 4.0.

flatten the beam ion distribution function. The simulations also showed that changes in resonant particle perpendicular and parallel energies can be several times larger than their total energy change, implying that even relatively small amplitude modes can significantly modify the beam distribution in the resonant region and thus impact the instability drive and heating effectiveness. Moreover, the presence of multiple unstable modes led to the fastest growing mode flattening the beam ion distribution, which subsequently reduced the amplitudes of subdominant modes, demonstrating the importance of including all unstable toroidal mode numbers in the nonlinear simulations for accurate estimates of mode amplitudes needed for transport studies. The presence of a second more tangential neutral beam in NSTX-U compared to NSTX will allow to use fast ion phase space engineering to attempt to suppress the GAEs and CAEs.

2.1.3. Role of micro-instabilities. Micro-instabilities, and in particular those driven by electromagnetic effects, were identified as significant contributors to electron heat transport and T_e flattening. It was found that incorporating the parallel magnetic field fluctuations $\delta B_\parallel$ in CGYRO [26] simulations of high-performance NSTX discharge (shot 133964, with high sustained poloidal β) [27] significantly increases predicted growth rates and can lead to a shift in the dominant instability from microtearing modes (MTMs) to Kinetic Ballooning Modes (KBMs) [28]. KBMs, characterized by their large growth rates, were identified as a potential driver of electron temperature flattening because they can rapidly transport heat across flux surfaces. It was found that experimental NSTX profiles were often near the onset of KBM-driven transport, and that predictive TGYRO [29] modeling including $\delta B_\parallel$ significantly improves the accuracy of temperature profile predictions in high-beta NSTX plasmas. The improvement in the accuracy of the predicted ion (T_i) electron temperature profiles in NSTX high-beta plasmas when the $\delta B_\parallel$ effects are included is shown in figure 2. Without $\delta B_\parallel$, the T_e profile is significantly over-predicted, while with the inclusion of $\delta B_\parallel$, the predicted T_e profile is brought much closer to the experimental levels, and the predicted gradients are flatter, which is more consistent with the experiment.

The importance of incorporating $\delta B_\parallel$ effects in understanding T_e flattening is further underscored by separate global nonlinear electromagnetic gyrokinetic simulations of projected low collisionality and high-performances NSTX-U discharges [30]. Self-generated zonal flows were found to be crucial for regulating KBM-driven turbulence, breaking up large turbulent eddies, reducing their radial correlation length, and decreasing turbulent transport. The presence of compressional magnetic field fluctuations was shown to be essential for destabilizing the KBM, and their amplitude to be comparable to transverse fluctuations, a feature distinct from conventional tokamaks.

Moreover, studies on the saturation mechanisms of MTMs demonstrated that the effectiveness of $E \times B$ shear in suppressing MTM-driven transport highly depends on the magnetic shear ($\hat{s}$) and the ballooning angle dependence of the MTM linear growth rate [31]. At high magnetic shear the distance between rational surfaces is reduced, which causes the MTM-driven magnetic islands to overlap, creating significant stochastic transport, whereas at low magnetic shear there is little stochastization. In NSTX-like plasmas, towards the core-edge boundary where $\hat{s}$ is large, it was shown that $E \times B$ shear can reduce electron heat flux by more than an order of magnitude by enhancing coupling between unstable and stable modes. This indicates that while MTMs can drive electron heat transport, sufficiently strong $E \times B$ shear can effectively mitigate this form of flattening. The possibility of having two neutral beams in NSTX-U, each with three different sources, will allow great flexibility in modifying the rotation profile, and therefore allow to investigate the use of $E \times B$ shear to prevent the flattening of the T_e profile.

2.2. Progress in understanding pedestal transport and stability

Understanding pedestal transport is paramount for optimizing high-performance plasma operation, as the pedestal acts as an edge transport barrier that significantly impacts

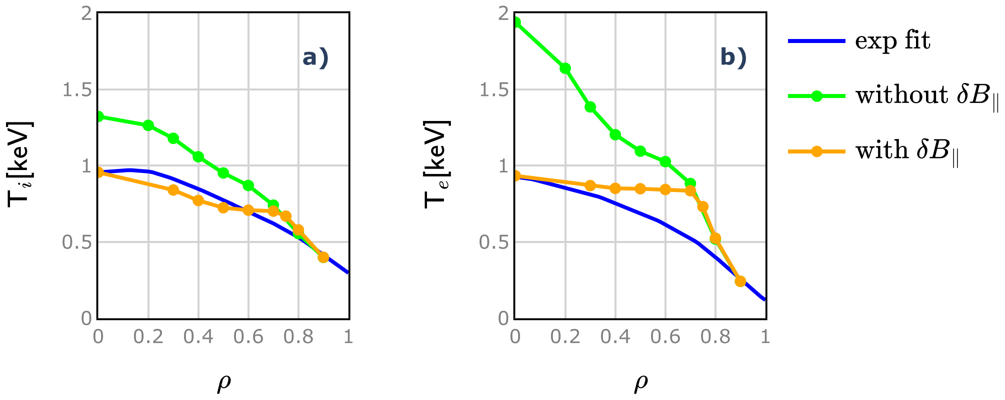

Figure 2. TGYRO prediction of NSTX discharge # 133964 at $t = 800$ ms without $\delta B_\parallel$, and with the inclusion of $\delta B_\parallel$. The blue solid lines are the experimental fits. Reproduced from [28].

core confinement and, consequently, fusion power production. While conventional models like EPED [32] have successfully predicted pedestal structure in many conventional aspect-ratio tokamaks, they have shown limitations in low-aspect-ratio devices like NSTX, where observed pedestals are notably wider than predicted [33].

Recent studies have made significant strides in understanding pedestal transport in NSTX and NSTX-U, particularly by demonstrating that KBMs, not ideal-ballooning modes, are the primary instabilities limiting achievable confinement in ST pedestals [34, 35]. This finding is central to the Gyrokinetic Critical Pedestal (GCP) model—a linear gyrokinetic threshold model used for pedestal width and height scaling prediction—which accurately predicts the steepest pressure profiles a pedestal can sustain under the influence of gyrokinetic instabilities [36]. By combining linear gyrokinetics with self-consistent equilibrium variations, the GCP model achieves excellent agreement with experimental pedestal width-height measurements in NSTX, such as discharge 139047, where the KBM clamps the pedestal profiles at experimentally observed values, notably below the ideal-ballooning stability boundary. Furthermore, a novel bifurcation in KBM stability was observed. Such bifurcation leads to the existence of two distinct pedestal branches: a wide and a narrow branch, both of which have been accessed in NSTX experiments [37]. This bifurcation, and consequently the pedestal width-height scaling, were found to be strongly dependent on plasma shaping (elongation κ, triangularity δ) and aspect ratio.

The role of equilibrium flow shear was also investigated as an additional constraint on pedestal evolution and a potential saturation mechanism for pedestal growth. Comparing a standard ELMy NSTX H-mode (139047) with a wide pedestal, ELM-free discharge (132588), the latter is shown to possess significantly stronger pedestal top flow shear. While the general expectation is that flow shear suppresses turbulence [38], its efficacy in discharge 139047 initially decreases with increasing width, before increasing at larger widths, suggesting a complex interplay where flow shear can impose an additional constraint on the achievable pedestal width and height by mediating the effective transport levels. The combined effects of KBM stability, flow shear, and transport delineate a relatively narrow window of accessible pedestal operating space, as it can be seen from the cartoon in figure 3.

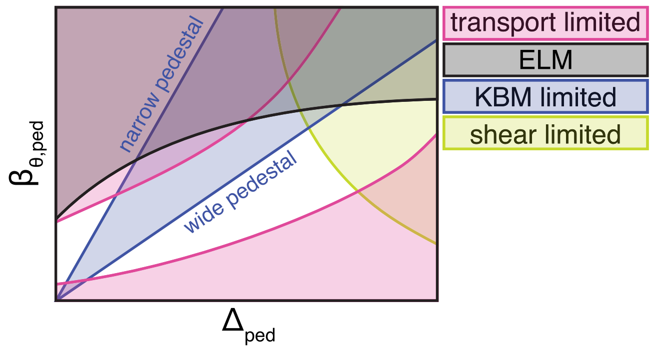

Figure 3. Cartoon showing the combination of GCP stability, flow shear, transport, and ELM constraints on a plot of $\beta_{\theta,\mathrm{ped}}$, the pedestal height in electron beta, vs. Δ_{ped}, the pedestal width in normalized poloidal flux. The color blocks indicate the excluded regions for a constraint curve of the same color. Accessible pedestal regions are those without any constraints. Reproduced from [37].

The impact of non-ideal effects like resistivity, plasma flow, and two-fluid physics on ELM stability, was also studied using the extended MHD code NIMROD [39]. It was found that toroidal rotation has a strong destabilizing effect, reducing the ELM onset threshold and shifting the most unstable modes to intermediate toroidal mode numbers. Conversely, two-fluid effects, including ion diamagnetic drifts and gyroviscosity, provide a significant stabilizing force that counteracts the flow-driven instability, especially for high-n ballooning modes. The role of resistivity was found to be more complex, since it is generally destabilizing for the ELM-free discharges studied, but can be stabilizing in other high-collisionality regimes. This suggests that a comprehensive model including all these competing effects is necessary for accurate ELM prediction and control.

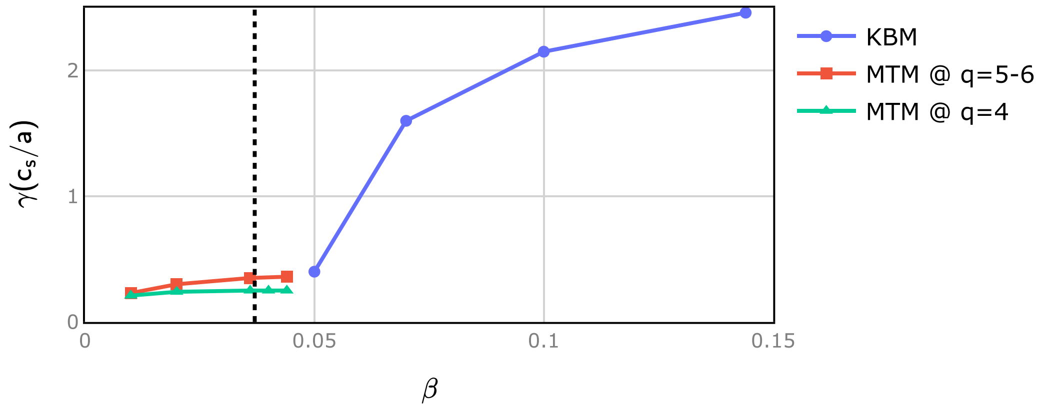

Figure 4. β scan of NSTX discharge 132588 calculated with the GENE code, showing an MTM to KBM transition. The experimental β value is shown by the dashed vertical line, 20% below the global critical KBM threshold. Reproduced from [43].

In addition, the study of the impact of the plasma resistivity on peeling–ballooning (PB) stability thresholds, was then extended to also include other STs like the Mega Ampere ST (MAST) and MAST-Upgrade (MAST-U) [40]. Using M3D-C1 it was found that resistivity destabilizes PB modes and significantly expands the unstable domain in both NSTX and MAST-U. The observation of resistive PB modes coincides with higher magnetic shear in the pedestal region. While MAST discharges were limited by ballooning modes and well-described by ideal-MHD, MAST-U exhibited resistive PB modes similar to those in NSTX, although with more dominant ballooning features. For MAST-U, ideal-MHD shows the plasma to be stable to PB modes in ELMing discharges, but including Spitzer resistivity renders the plasma unstable, aligning the model with experimental observations. Analysis of a DIII-D discharge with NSTX-like parameters found that its stability is governed by ideal PB modes, unaffected by resistivity. These comparisons suggest that magnetic shear in the pedestal region is the key factor linked to the emergence of resistive edge modes, rather than ST-typical plasma shape, temperature, or resistivity profiles alone.

Finally, electron temperature gradient (ETG) driven turbulence in the pedestal region was studied using electron-scale gyrokinetic simulations (CGYRO and GENE [41]) to compare non-lithiated (narrow pedestal, 132543) and lithiated (wide pedestal, 132588) discharges. It was found that, for the non-lithiated case, retaining $\delta B_{\|}$ in simulations revealed a new, strongly unstable branch of ETG modes at the pedestal top [42]. This branch leads to a substantial increase in electrostatic electron heat flux, which is otherwise negligible when $\delta B_{\|}$ is omitted. This strong ETG transport was found in the only region of the plasma where the pressure gradient is well below the kinetic ballooning mode limit, suggesting that electromagnetic ETG turbulence may be constraining the profile in this area. This $\delta B_{\|}$ effect is most pronounced for modes with strong toroidal magnetic drift resonance, which are favored by NSTX's high magnetic shear. In contrast, for the lithiated case, ETG transport is negligible at the pedestal top but becomes significant in the steep-gradient region, where $\delta B_{\|}$ plays a much weaker role but, when retained, can restore the stabilizing effect lost under the $\delta B_{\|} = 0$ approximation.

Analysis of the same wide pedestal and ELM-free NSTX discharge with the GENE code showed that, while the plasma was KBM stable, global MTMs were the dominant unstable long wavelength modes in the wide pedestal, as shown in figure 4 [43]. Two distinct branches of unstable MTMs were identified, one that grew at the pedestal top and another that grew within the pedestal. The frequencies of these simulated MTMs were found to be in good agreement with quasi-coherent fluctuations measured experimentally. These MTMs exhibited large radial extensions reaching deep into the core, suggesting their potential for global coupling and impact on core profiles through enhanced electron heat transport. Carbon impurities were found to play an important role in MTM stability. Neglecting them would result in an about 50% error in the growth rate calculations.

2.3. Development and validation of reduced or surrogate models

High-fidelity, first-principles simulations, such as those performed by gyrokinetic codes or comprehensive transport suites like TRANSP [44], are often computationally intensive, requiring hours or even days to complete. This computational burden renders them unsuitable for real-time control, rapid scenario optimization, or between-shot analysis. Therefore, there is a need for faster, yet accurate, models that can capture the complex physics of low-aspect-ratio, high-beta STs where turbulence characteristics and transport mechanisms can significantly differ from conventional devices. The work done to address this challenge in the last two years is summarized below. Overall, these efforts demonstrate significant progress in providing robust, validated, and computationally efficient reduced and surrogate models crucial for understanding and controlling pedestal transport and broader plasma behavior in NSTX and NSTX-U.

2.3.1. Progress in the development of surrogate models. MMMNet, a neural-network (NN)-based surrogate model for the Multi-Mode Module (MMM) [45], specifically trained on NSTX-U experimental data, was introduced [46]. This model

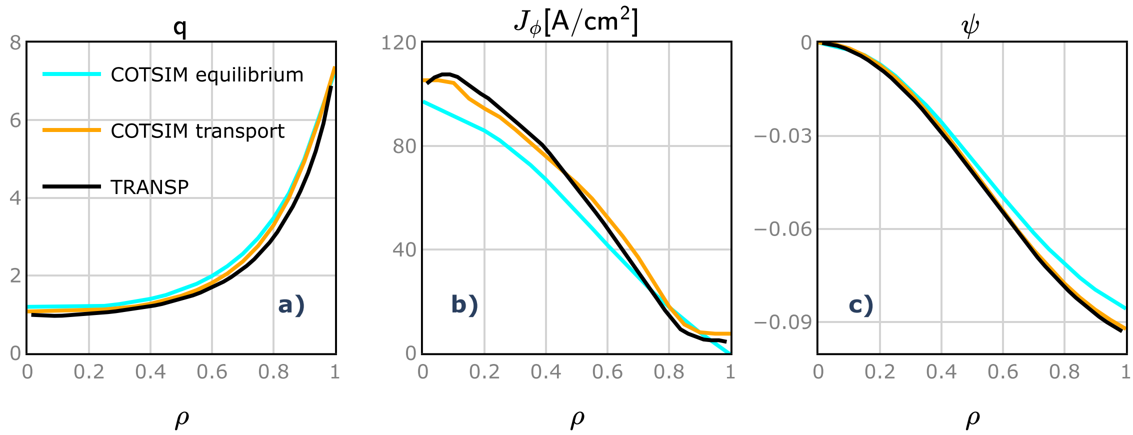

Figure 5. Comparison of safety factor (*a*), toroidal current (*b*) and magnetic flux (*c*) radial profiles computed with COTSIM and TRANSP. Reproduced from [51].

predicts various diffusivities (thermal, particle, momentum) with similar accuracy to MMM but runs two orders of magnitude faster.

At the same time a new version of MMM with significantly improved computational efficiency, essential for applications such as scenario optimization, has been developed [47]. This updated version incorporates advanced physics in its reduced models, including MTMs and a new electromagnetic ETG mode (ETGM [48]), both of which are critical for low-aspect-ratio, high-beta tokamaks. The model has been shown to be consistent with gyrokinetic simulations (CGYRO) and is capable of predicting electron and ion temperature profiles in NSTX.

Moreover, the Control-Oriented Transport SIMulator (COTSIM), an integrated equilibrium and transport simulation framework was also enhanced. COTSIM incorporates NN-based surrogate models for both MMM (MMMNet) and NUBEAM (NUBEAMNet) [49, 50] to predict anomalous diffusivities and NBI source depositions, respectively [51]. By coupling these with self-consistent equilibrium calculations, COTSIM was able to achieve strong agreement with TRANSP predictions, as shown in figure 5 for NSTX-U discharges, while significantly reducing computation time, making it a robust tool for real-time profile estimation, scenario optimization, feedback control design and testing, and integration into digital twin frameworks.

A data-driven electron thermal transport NN (ETT-NN) model for NSTX was also introduced [52]. Validated against TRANSP and predictive TRIASSIC [53] simulations, ETT-NN was shown to accurately reproduce electron temperature trends and exhibits physically consistent responses to parameter scans for various turbulent modes (MTM, ETG, KBM), demonstrating its ability to reflect underlying physical characteristics without explicit theoretical background.

Multiple machine learning surrogate models, including random forest regressors (RFR), multilayer perceptron (MLP) regressors, and Gaussian process regressors (GPR), have been developed for ion cyclotron range of frequencies (ICRF) heating predictions in NSTX [54–56]. These models achieve six orders of magnitude acceleration compared to the full-wave solver TORIC [57] while maintaining high accuracy. A key contribution was the identification, diagnosis, and correction of a numerical instability in the legacy TORIC code for the high-harmonic fast wave (HHFW) regime. By using both a curated dataset and an outlier-free dataset, the trained surrogates were shown to accurately capture the physical HHFW heating profiles. Particularly, through physics-informed data curation and appropriate selection of model families (RFRs and GPRs), it was demonstrated that accurate generalization to unseen regions of parameter space is possible, providing an alternative solution for predictions in challenging regimes where original data/model is not reliable but the underlying physics regime still holds. GPRs also provide calibrated uncertainty quantification, which enhances reliability and interpretability. Newer models and workflows remove the two main bottlenecks in surrogate deployment: data ingestion and analysis, and hyperparameter tuning. Automated data pipelines and Bayesian hyperparameter optimization establish an end-to-end, reproducible surrogate implementation methodology, which is being employed to develop surrogates for other fusion-relevant applications, including MHD stability prediction and gyrokinetics.

2.3.2. Progress in validation of reduced models. Validation of reduced models against linear and nonlinear gyrokinetic simulations using the fully electromagnetic high-fidelity code CGYRO were performed. In a comparison between the trapped gyro-landau fluid (TGLF) [58] and the new gyro fluid system (GFS) [59] codes, it was demonstrated that GFS shows significantly better agreement with CGYRO than TGLF, particularly in capturing the destabilizing effect of parallel magnetic fluctuations on KBMs, a crucial step for improving reduced models for future transport predictions and control in STs [60].

In an effort to analyze ETG stability and thermal transport in NSTX and NSTX-U plasmas, CGYRO results were also compared with predictions from the ETGM and the TGLF model, emphasizing that while ETGM shows power flow close to experimental values and CGYRO results, TGLF with

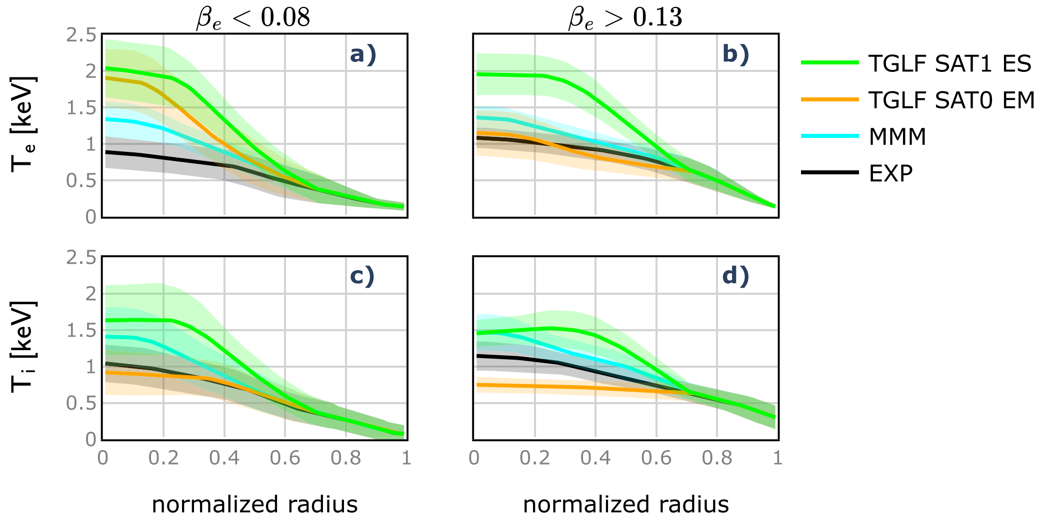

Figure 6. T_e—in (*a*) and (*b*) - and T_i—in (*c*) and (*d*) - profiles averaged over several NSTX discharges with low—a) and (*c*) - and high—b) and (*d*) - β values. In black the experimental value, in color the TRANSP results using several models [63, 64]. Reproduced from [63].

saturation rule SAT0 tends to underpredict the power flow from ETG modes [61]. Discrepancies in growth rate trends and thresholds between CGYRO and the reduced models were also noted, indicating areas for further investigation.

The capabilities of the MMM and the TGLF reduced turbulent transport models in reproducing experimental temperature profiles from a large set of high-performing NSTX discharges was also evaluated [62, 63]. Overall, MMM was found to provide more robust and computationally efficient predictions, consistently agreeing with experimental data better than TGLF within time-dependent, predictive TRANSP simulations. MMM typically overpredicted the electron and ion temperature profiles by about 15%–40% and 20%–35% respectively, and closely reproduced the observed T_e/T_i ratio of $\sim 0.9-1$. In contrast, electromagnetic TGLF simulations were more sensitive to plasma β, more substantially overpredicting T_e at relatively low β and underpredicting T_i at higher β, yielding an elevated T_e/T_i ratio relative to the experimental value, as can be seen in figure 6. Moreover, MMM's predictions tended to be more reliable for discharges with higher β, longer energy confinement times, and broader temperature profiles. The dominant transport mechanisms predicted by MMM varied radially and with plasma conditions: ETGMs dominate near the core, kinetic ballooning and trapped electron modes become important at mid-radius in high-β, low-collisionality plasmas, and MTMs drive transport near the pedestal, especially at high β.

2.3.3. Progress in equilibrium reconstruction. Accurate MHD equilibrium reconstructions are crucial for stability and transport analysis. An approach that integrates the EFIT equilibrium solver with experimental data analysis and TRANSP simulations to enhance NSTX and NSTX-U equilibrium reconstruction accuracy, particularly at the edge, was developed [65]. This is achieved by adding constraints on total pressure and current density profiles based on the TRANSP solutions. The accuracy depends on the availability and quality of experimental measurements, data consistency between various constraints, and choice of basis functions to represent the pressure and current density profiles. Improved fidelity in equilibrium reconstruction obtained with this new integrated method was observed, with reduced variability of magnetic axis and boundary locations from several centimeters to millimeters, and q_0 variability reduced tenfold. The impact of equilibrium reconstruction on plasma profiles (electron temperature, density, ion temperature, rotation) through mapping experimental measurements to flux coordinates was analyzed, showing significant effects, especially at the edge due to strong flux suppression near the last closed flux surface.

3. Power & particle handling for plasma exhaust in high performance scenarios

This objective aims to develop power exhaust techniques for NSTX-U integrated scenarios and evaluate their extrapolability to future devices, as well as to develop particle control techniques to enable NSTX-U integrated scenarios. With increased heating power and compact geometry, NSTX-U will produce very high peak heat fluxes (up to $\sim$100 MW m^{-2}), requiring the development of robust solutions at the Plasma–Material Interface (PMI). This includes assessing the performance and lifetime of new PFCs like castellated, fish-scaled graphite tiles, developing mitigation techniques such as advanced magnetic configurations (e.g. snowflake divertors) and radiative solutions, and exploring innovative liquid lithium (LL) PFCs.

3.1. Liquid lithium plasma-facing components

LL is being explored as a promising solution for the challenges of power and particle handling in high-performance fusion devices. It offers a renewable plasma-facing surface that

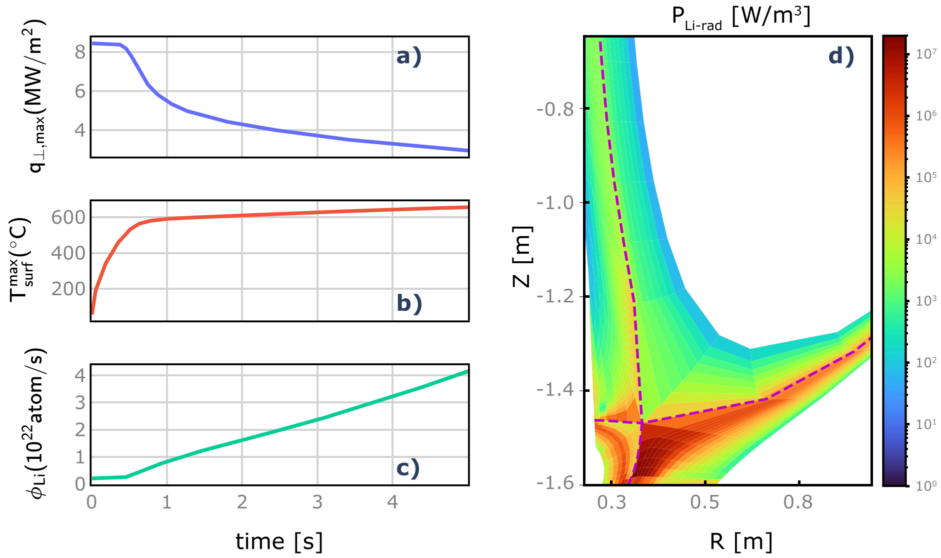

Figure 7. On the left, time evolution of the maximum surface heat $q_\perp$ (*a*), temperature (*b*) and lithium source rate (*c*). On the right (*d*) a 2D map of the power density radiated by lithium at $t = 5$ s. Reproduced from [67].

can significantly enhance power exhaust, protect the solid substrate, and potentially improve energy confinement through the pumping effect achieved by its chemical bonding with hydrogen isotopes. Furthermore, LL can act as a carrier of heat energy and, crucially, as a vapor shielding material when evaporated, which aids in heat flux redistribution.

A new self-consistent, time-dependent modeling framework that couples the plasma boundary transport code UEDGE [66] with a new lithium wall transport code, Wall-Li, was developed to evaluate the performance and operational limits of LL divertors [67]. Applied to an NSTX-like geometry, the model was used to simulate how lithium is sourced from PFCs based on local plasma conditions and surface temperature. It was found that a lithium vapor shielding acts as an effective self-regulating mechanism for mitigating divertor heat flux; when the PFC surface temperature exceeds 450°C, lithium evaporation becomes the dominant sourcing mechanism, leading to significant radiative power losses that reduce the peak heat flux and cause the surface temperature to saturate near 600 °C (see figure 7). While this protects the divertor, it also increases lithium concentration in the upstream plasma, potentially leading to core fuel dilution. Strong main ion parallel flow is found to be critical for confining lithium within the divertor region, thereby reducing core contamination. This suggests that managing plasma flow could be a key strategy for optimizing lithium-based PFCs in future devices.

Development and analysis of a new variant of PFCs called the Capillary Porous System with Fast Flowing LL (CPSF) were also carried out [68–70]. This innovative design incorporates a porous wall to stabilize the liquid metal surface, while a MHD drive pushes the LL flow inside the component, ensuring efficient heat exhaust and enhanced control of the LL surface temperature. A key advantage of this system is its inherent self-regulating feedback effect: as heat flux increases, the evaporation rate of lithium rises, and as heat flux decreases, the evaporation rate falls, which can create a protective vapor shield around areas of peak heat flux. Utilizing CPSF as an evaporator for vapor shielding allows handling significantly higher divertor heat fluxes compared to previous designs, while still avoiding high lithium concentrations in the core. To accurately model this complex system, a two-way coupling between plasma-edge analysis and PFC heat transfer analysis is essential. To do this, SOLPS-ITER [71] was used coupled with an analytical slab flow model for heat transfer within the PFC. These analyses have shown that increasing the LL flow velocity or decreasing the initial LL temperature consistently leads to a reduction in lithium-ion concentration in the plasma core and lower total lithium evaporation from the divertor by influencing the divertor wall temperature upstream. Another finding is that deuterium gas puffing can significantly reduce lithium concentrations in the core, achieving effective screening of lithium due to an increased friction force that pushes lithium towards the target. Furthermore, it was observed that the flow direction of LL is critical, with flow towards the Private Flux Region (PFR) generally yielding lower core lithium concentrations compared to flow from the PFR.

Further optimization studies have explored the best locations for lithium evaporation and the ideal PFC geometries [72, 73]. Initial comparisons revealed that PFR evaporation is significantly more efficient at dissipating power and reducing peak heat flux, requiring lower gross lithium evaporation rates and resulting in lower upstream lithium concentrations, primarily due to its improved access to the separatrix. Building on this, the ‘lithium vapor box’ design was simplified into a ‘lithium vapor cave’ by removing the common flux region baffles, as the plasma itself acts as a ‘virtual baffle’ to contain neutral lithium. Simulations demonstrated that making selected surfaces reflective to lithium (such as the cave walls and target walls) can drastically reduce the required net

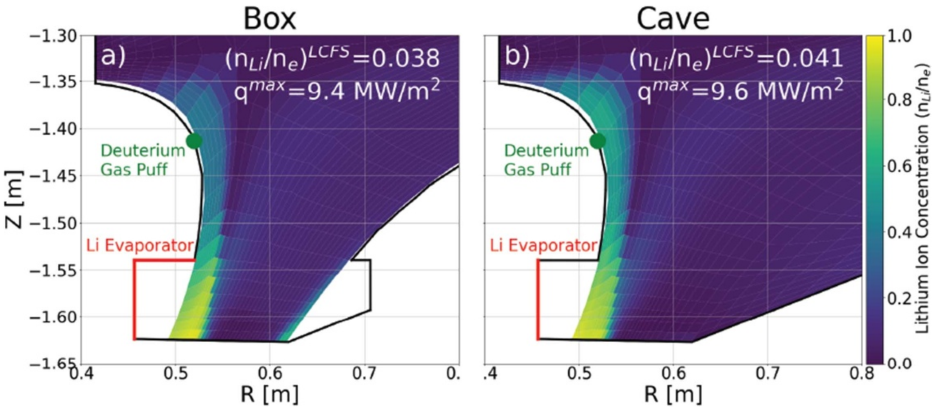

Figure 8. Lithium concentration predictions for the box (*a*) and the cave (*b*) geometries [72].

lithium evaporation rate (by orders of magnitude) and decrease the minimum upstream lithium concentration. This is because reflection directs lithium flow towards the plasma and promotes recirculation, leading to multiple ionizations per evaporated lithium atom. While cave depth and aperture height have minor effects on upstream concentration, the shaping of the PFR structure was found to have a more significant impact, influencing how lithium contamination occurs and whether the X-point acts as a source or sink for the confined region. Additionally, the poloidal location of deuterium puffing in the PFR can impact performance, with positions near the deuterium flow reversal point resulting in improved lithium containment via increased friction force acting on the lithium. An important finding is that the differences in performance between various PFC geometries are minimized when drifts are enabled, as the flows become dominated by drift terms, suggesting increased design flexibility. A comparison between the box and cave geometries in terms of lithium concentration in the plasma is shown in figure 8.

Preliminary engineering design work of a PFR lithium evaporator has focused on the evaporator's heating and cooling characteristics during the plasma pulse cycle, with particular focus on how the temperature of the evaporator can be controlled to maintain a constant rate of evaporation over a 5 s plasma pulse, and how to minimize the amount of lithium consumed between plasma pulses on a 20 min cycle [74]. It was found that—since the plasma radiation impinging on the divertor surfaces plays a key role in the total power balance of the system—controlling the lithium evaporation rate during the plasma pulse requires either active cooling of the divertor surfaces or the use of baffling to protect the lithium evaporator from the divertor radiation. Accordingly, a new conceptual design was presented where the lithium evaporator was moved out of the line-of-sight of the plasma radiation so that the power balance of the evaporator is dominated by embedded heaters, and a hot, reflecting surface was used to direct the flow of lithium vapor from the evaporator to the divertor plasma. It was found that before the pulse, high power-density heaters are needed to ramp up the temperature of the evaporator to the desired operating point as quickly as possible, while after the plasma pulse, the heaters could be turned off and the evaporative cooling effect of the lithium would naturally limit the amount of lithium consumed by the evaporator.

3.2. Plasma edge transport, dynamics, and modeling

Research was also focused on the intricate physical processes that govern plasma behavior in the scrape-off layer (SOL), including the dynamics of turbulent structures like blobs, the critical role of neutral particles in transport, and the development of computational models to understand core-edge interactions.

Filamentary structures in the SOL naturally emerge from edge plasma turbulence, driving intermittent particle and heat transport that can degrade confinement and impose high heat fluxes on PFCs. These plasma filaments—also known as blobs - were analyzed using the gas-puff imaging (GPI) diagnostic [75]. A watershed-based method was developed to identify, segment, and track blob contours in successive GPI frames, allowing characterization of their shape evolution, velocity, and rotation [76]. Results showed that larger blobs tend to be less circular and more concave, consistent with theoretical predictions of increased instability in larger structures [77, 78]. A positive correlation between radial position and velocity suggested outward acceleration, possibly due to reduced viscous drag toward the far SOL. Unlike ELM filaments, which exhibit strong rotation [79], SOL blobs display minimal spin. Statistical analysis of solidity and curvature revealed broad, near-Gaussian distributions, indicating stochastic shaping by background turbulence. Comparisons with plasma profiles further revealed dependencies between blob rotation, poloidal velocity, collisionality, and line-integrated density, providing new constraints for validating SOL transport and turbulence models.

The influence of neutral interaction on the SOL was investigated, with particular attention to turbulence, parallel transport, and the dynamics of plasma blobs [80]. Using a continuum gyrokinetic code coupled with a kinetic neutral transport model, it was observed that the presence of neutrals results in flatter density profiles due to changes in parallel transport, underscoring the importance of neutral drag on global plasma properties. Blobs were observed to be, on average, slower and larger in simulations that include neutrals compared to those without, and it was also observed that charge exchange collisions are crucial for accurate modeling of parallel transport. While blob motion did not significantly contribute to radial transport in these simulations, it was necessary to include neutral dynamics in turbulence models to accurately predict blob behavior and their role in determining the SOL width. Comparing simulations with a full neutral model against those with an effective ionization source it was possible to separate the effects of particle sourcing from collisional drag. This revealed that many profile differences could be accounted for by ionization sourcing. However, the density profile flattening could not be reproduced from sourcing alone and was attributed to slower parallel plasma flow from charge exchange collisions.

A reduced model for the SOL plasma called SOL Box model, designed for core-edge integrated scenario modeling, was introduced [81]. The 0D Box model is based on global power and particle balance and aims to capture essential SOL transport physics with minimal computational cost, making it suitable for wide parameter-space exploration in FPP design. It extends the conduction-limited two-point model by incorporating a free parameter for the divertor particle recycling rate and can reproduce plasma limiting behaviors from sheath-limited to conduction-limited regimes. A 1D extension that account for parallel variations of plasma parameters along magnetic field lines, was compared against SOLPS-ITER simulations of an NSTX ELM-free H-mode discharge with solid lithium-coated divertors. The 1D model, formulated with analytical approximations for power loss, flux expansion, and ionization sources, produced satisfactory results for electron temperature and density compared to SOLPS, especially for upstream density, despite discrepancies near the target where strong convective transport exists in SOLPS.

3.3. Divertor power exhaust, management, and control

As already mentioned, the effective management of high heat flux on plasma-facing components is a critical challenge for the development of fusion reactors, as excessive heat can lead to component damage and reduced operational lifetimes. Understanding and predicting these heat loads, including in the presence of magnetic perturbations, is essential for machine protection and the design of future fusion devices.

One approach to tackle this problem involved improving the tools for heat flux assessment and exploring new divertor configurations. The open-source, Python-based code HYPERION has been developed to accurately calculate heat flux incident on PFCs using infrared thermography data [82]. This 2D implicit finite-difference code is noted for its accessibility and ability to optimize mesh thickness and account for thin surface layers on PFCs. HYPERION has shown excellent agreement with established heat flux codes like THEODOR [83] and good agreement with TACO [84], thereby enhancing confidence in its utility for machine protection and power balance accounting.

Beyond measurement, mitigation strategies were explored through the Snowflake (SF) divertor configuration, which aims to provide a more effective solution to power exhaust [85]. This configuration creates a second-order poloidal field null, theoretically offering benefits such as higher flux expansion and extended PFRs, which are beneficial for achieving a stable X-point radiator (XPR) regime - a regime characterized by significant radiated power loss, leading to divertor power detachment, while maintaining good or only slightly degraded core confinement. Experiments in NSTX with SF divertors demonstrated many XPR features, including good confinement, and substantial divertor power detachment.

Further investigations into heat flux phenomena have revealed the complex nature of heat distribution on divertor plates, particularly in the presence of Resonant Magnetic Perturbations (RMPs). Previously, striated heat fluxes with RMPs were mainly attributed to strike point splitting caused by magnetic lobe structures intersecting the divertor. However, recent observations in NSTX have identified the presence of stationary 3D filaments induced by $n = 3$ RMPs [86]. These filaments remain fixed toroidally and extend from the midplane to the divertor suggesting that these stationary filaments are the primary cause of the divertor heat flux striations with RMPs in NSTX, challenging the previous understanding that relied solely on strike point splitting. These stationary filaments were also found to reduce the divertor peak heat flux. This new understanding of filament-induced heat transport is crucial for controlling the peak divertor heat flux in NSTX-U. Figure 9 shows images of the filaments from a visible camera and heat fluxes at the divertor from an infrared one.

4. Developing steady-state non-inductive and low-disruptivity operations

The core deliverable for this objective is to achieve high-beta non-inductive scenarios that integrate good energy confinement, low disruptivity, and suitable heat flux mitigation in stationary conditions. To progress toward this goal, research has been focused on scenario development, real-time capabilities and disruption forecasting and avoidance.

4.1. Progress in scenario development

Developing steady-state non-inductive scenarios is paramount for realizing economically viable fusion energy. Traditional tokamak operation relies on inductive current drive, which is inherently pulsed, limiting the duration of plasma discharges and preventing continuous energy production. Achieving steady-state operation requires that the plasma generate and sustain its own current non-inductively, primarily through self-driven mechanisms like the bootstrap current, supplemented by external non-inductive current drive methods such as high harmonic fast waves and NBI. Furthermore, optimizing confinement and maximizing fusion power output are crucial for reactor economics. However, challenges like magnetic instabilities and complex interactions between heating and current drive systems must be addressed to ensure stable and efficient long-pulse operation.

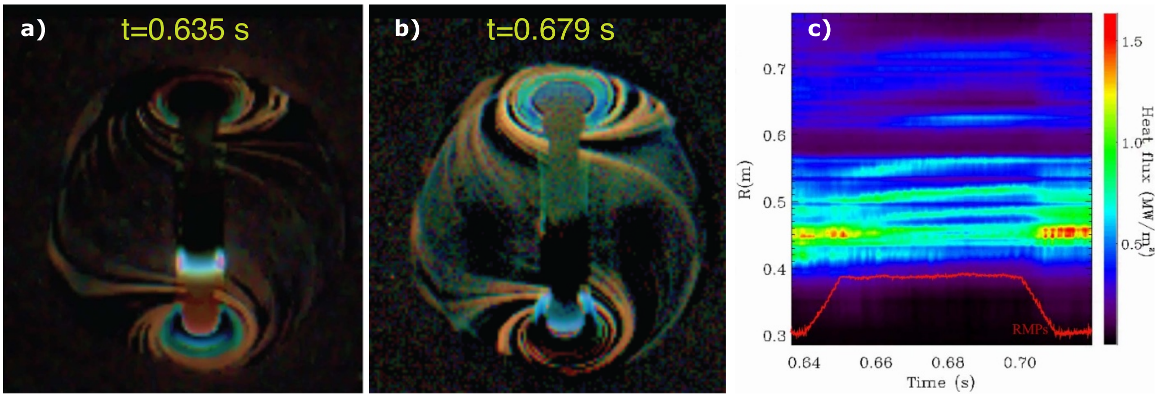

Figure 9. Images of the filaments before (*a*) and after (*b*) $n = 3$ RMP application and consequent heat fluxes at the divertor (*c*) in NSTX discharge 134779. Reproduced from [86].

RMS is a key plasma configuration known to suppress electron thermal transport and lead to the formation of internal transport barriers (ITBs), which significantly improve energy confinement and result in increased temperature and peaking of the pressure profile. Through studies done with TRANSP it was observed that RMS in NSTX-U can be generated through a fast current ramp and early neutral beam injection into a large plasma volume, a method successfully used in both the Tokamak Fusion Test Reactor (TFTR) [87] and NSTX [88]. Furthermore, it was shown that sustaining RMS and keeping the minimum safety factor $q_{\min} > 1$, to avoid potential $q = 1$ driven MHD events, can be achieved by increasing the core electron temperature, either via increased plasma current and/or adding heating power. This is vital for maintaining the improved confinement properties over long pulses. While the new off-axis NBI sources did not dramatically change the q-profile in simulations with rigidly scaled profiles, the results provide a predictive framework and operational strategies for shaping the q-profile to enable and sustain high-performance, non-inductive operation in NSTX-U.

A critical challenge for achieving steady-state, high-performance operation is the avoidance of MHD instabilities like neoclassical tearing modes (NTMs), which can degrade confinement and lead to disruptions. Using a TRANSP-based model of the modified Rutherford equation, a detailed analysis of several NSTX discharges featuring spontaneous (2,1) NTMs revealed that fast ions play a critical role in the early growth phase of the instability [89]. The 'kinetic neoclassical' polarization current, driven by fast ions, is found to disrupt the marginal stability of the plasma and allow the magnetic island to grow. Furthermore, M3D-C1-K [90] simulations suggested that fast ions may also contribute to the NTM onset by increasing the total plasma pressure enough to excite a pressure-driven ideal mode, which can then provide the necessary seed island for the NTM.

The presence of non-axisymmetric magnetic fields due to coil misalignments and manufacturing imperfections (known as error fields) is another factor that can significantly affect plasma performance in tokamaks. Their impact is typically assessed using perturbative MHD models. The validity of such an approach was investigated by comparing the results to fully 3D nonlinear equilibria generated by the VMEC code [91], in order to establish: the correct choice of the axisymmetric reference frame to use in perturbative calculations and the validity limits of the linearized theory [92]. It was shown that the appropriate reference frame is determined by the radial centroid of the toroidal field coils, as radial shifts of these coils shift the plasma's magnetic axis with them, while choosing the wrong frame can lead to significant errors in predicting the plasma response. It was also found that linear theory breaks down when coil misalignments exceed approximately 1% of the minor radius, which is larger than the tolerances of NSTX-U. These findings validate the use of perturbative codes for setting current NSTX-U tolerances, but highlighting that non-linear models may become necessary for future devices.

A novel effect impacting the self-driven current drive mechanism was revealed: magnetic-island-induced 3D electric potential structures, which have the same dominant mode numbers as the magnetic island but are centered at the inner and outer edges of the island [93]. These non-resonant potential islands are shown to drive a parallel current through an efficient nonlinear parallel acceleration of electrons. It was found that in large-aspect-ratio tokamaks, in addition to the well-known local current loss due to pressure profile flattening across the island, this effect can cause a significant global reduction of the bootstrap current once a critical magnetic island width is exceeded, with the loss increasing rapidly with island size. Conversely, for low-aspect-ratio STs like NSTX-U, the current loss caused by magnetic islands was found to be minor, primarily local to the island region, and the rate of current loss as the island size increases is substantially slower. In the reactor-relevant high-β_p regime, where NTMs are more likely to develop, the bootstrap current reduction in STs is found to be even smaller, as shown in figure 10. This work fundamentally reassures that magnetic islands may not be a major impediment to maintaining self-driven current in STs.

The role of high harmonic fast waves was explored as a versatile heating and current drive tool for NSTX-U scenario development. Utilizing the GENRAY [94] ray-tracing code coupled with the quasilinear Fokker-Planck code CQL3D [95], extensive parametric scans were performed to identify optimal conditions for HHFW current drive and

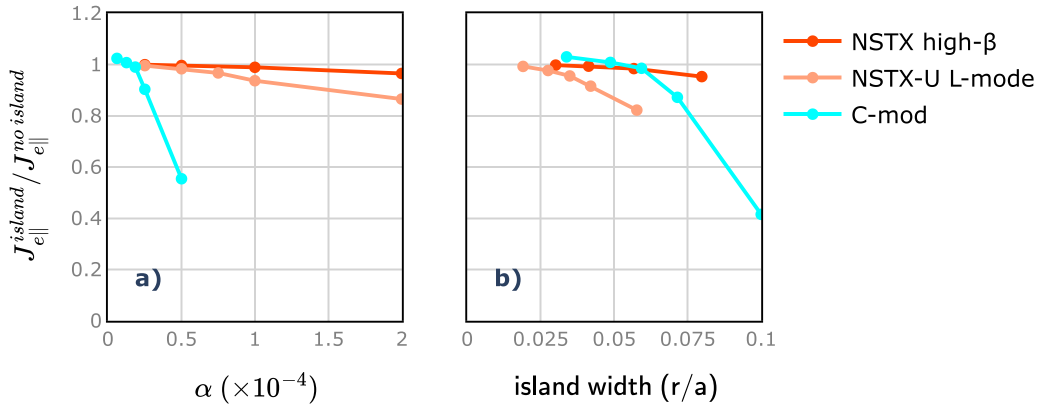

Figure 10. Total electron current with the presence of an island, normalized by the bootstrap current without an island as a function of: (*a*) the parameter α, proportional to the island perturbation amplitude δB; and (*b*), the island width (normalized by the minor radius). Three different plasmas from three different machines are shown [93]. Reproduced from [93].

heating [96]. The best current drive results were obtained at elevated electron temperatures and with the lowest toroidal wave number. The analysis quantified the HHFW current drive efficiency, demonstrating that at low densities, the efficiencies are high enough to support nearly fully non-inductive operation during the early ramp-up phase, aligning with previous NSTX results [97]. However, a significant finding was that adding neutral beams typically strongly reduces the HHFW current drive efficiency at low densities due to HHFW absorption on beam ions, which competes with electron absorption. This necessitates careful scenario development to weigh the benefits of beam-driven current against the potential loss of HHFW-driven current.

A significant challenge in using HHFW observed in previous NSTX experiments was that, under certain edge plasma conditions, up to 60% of the power could be lost in the SOL, never reaching the plasma core [98]. These losses were pronounced under the lower field, higher edge density conditions, where the fast waves were able to propagate in the SOL. To understand and overcome this issue, HHFW propagation in the NSTX-U SOL was modeled using a finite element approach in Petra-M [99], which solves the non-linear 2D heat conduction equation to derive 'anisotropy-resolved' density and temperature profiles, successfully capturing the effects of high parallel-to-perpendicular heat conduction anisotropy (up to $\chi_\parallel/\chi_\perp = 10^8$) that causes profiles to follow magnetic flux contours [100]. It was found that as the midplane density profile broadens, the wavefield intensity and its poloidal extent in the SOL are reduced. This broadening effectively reduces the gap width in front of the antenna, suppressing the excitation of geometry-dependent edgemodes (or waveguide modes), which in turn decreases the fraction of power deposited parasitically in the SOL and improves core coupling. In agreement with previous studies [101], the analysis suggests that higher field operation on NSTX-U is expected to mitigate parasitic edge losses, both by raising the fast wave onset density, thus prohibiting fast wave coupling to the SOL, and by lengthening the perpendicular wavelength, which would reduce the likelihood of parasitic SOL coupling even at high SOL density where the fast wave can propagate.

Finally—based on the possibility of increased core volume via plasma squareness ζ_0 that was observed in NSTX experiments [102]—a novel technique called 'volumetric power optimization' to enhance the fusion power output of magnetic confinement devices was presented [103]. The approach involves shifting the burning plasma region to a larger plasma volume by introducing minimal perturbations to the plasma boundary shape, specifically by varying ζ_0. It was shown that increasing ζ_0 can substantially increase total fusion power by more efficiently packing the burn volume, even with approximately constant power density profiles (see figure 11). The optimization was achieved while maintaining plasma stability, including vertical stability. The method offers operational advantages as it allows key plasma parameters like elongation and triangularity to remain unchanged while squareness is adjusted.

4.2. Real-time control

Advancing the capabilities of the NSTX-U plasma control system (PCS) is crucial for maximizing experimental performance, ensuring safe operation, and achieving high-performance plasma regimes in spherical tokamaks. This endeavor faces significant challenges, including the need to accurately predict and control complex, non-linear plasma dynamics, manage the inherent discrete nature and limitations of actuators like NBI, and mitigate common control issues such as plasma position oscillations and shape deviations that hinder access to desired operational modes. To address these challenges, several advances have been pursued.

One key development involves the creation and refinement of a virtual tokamak simulation platform, GSevolve, that allows the real PCS to control a simulated NSTX-U [104]. This capability is critical for off-line development and testing of control implementations and procedures, thereby saving valuable experimental time. The simulation has been rigorously

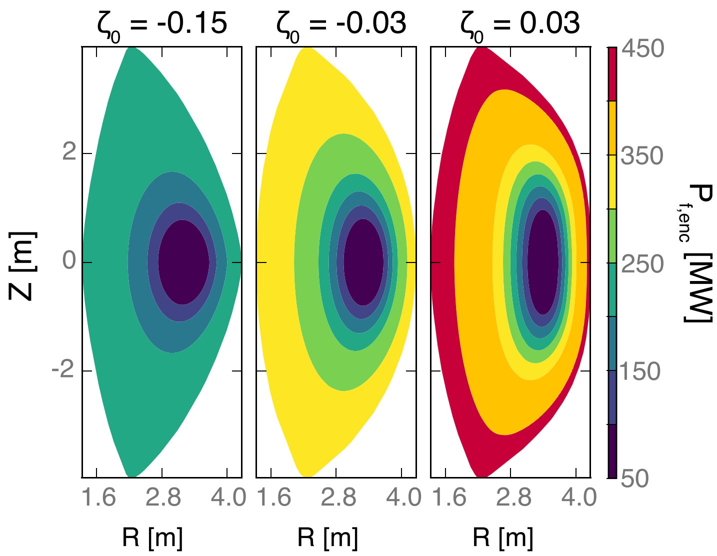

Figure 11. Integral of the fusion power density over the enclosed volume—also called 'enclosed fusion power' - in increasingly square plasmas for a hypothetical future ST pilot plant. Reproduced from [103].

upgraded to reproduce experimental profile evolution and outcomes at bifurcation points like vertical displacements, combining detailed 1D profile and 2D Grad–Shafranov equilibrium evolution. By integrating precomputed diffusion coefficients and heating/current drive profiles from the TRANSP code and allowing for iterative refinement, the fidelity of the simulation is significantly enhanced. Furthermore, it incorporates an implicit integration scheme, leading to an order-of-magnitude increase in simulation speed for NSTX-U, and an internal control system to facilitate debugging and testing of individual components. This virtual environment will play a vital role in designing and optimizing plasma ramp-up and full-shot scenarios for NSTX-U, with the goal of rapidly achieving high-performance plasmas.

The newly developed tokamak simulation platform has then been used to analyze and develop solutions for recurrent magnetic control problems, such as the 'bobble' phenomenon in NSTX-U [105]. The bobble consists of vertical oscillations and shape dithering during the plasma current ramp-up, which hindered reliable H-mode access and high performance during NSTX-U's first experimental campaign [106, 107]. By reproducing this complex behavior in simulations, it was identified that the bobble arises from a combination of the overall system's instability under feedback and significant input-output cross-coupling. To mitigate this, two primary control solutions have been proposed and tested: a modified two-stage I_p ramp-up trajectory and a Multi-Input Multi-Output (MIMO) decoupling controller. The modified I_p ramp-up trajectory, by temporarily flattening the current target during critical phases, aims to minimize control-loop interactions and had shown in simulations to reduce the amplitude of vertical oscillations by approximately 50%. The MIMO controller aims to enhance stability by reducing the vertical-instability growth rate and effectively decoupling control interactions, demonstrating in simulations that it can eliminate the vertical oscillations and maintain a more stable, double-null plasma shape, thereby enabling H-mode access and improved performance, as shown in figure 12.

Another significant area of advancement focuses on developing sophisticated control algorithms that explicitly account for the discrete nature of plasma actuators, particularly NBI systems. While the NBI power operates in an on/off Boolean style, conventional model predictive control (MPC) schemes often treat NBI power as a continuously varying signal, which is then converted to a discrete signal using pulse-width modulation. This signal conversion can lead to performance loss due to minimum on/off time constraints. To overcome this, a novel hybrid MPC algorithm has been designed for simultaneous regulation of the q-profile and stored energy in NSTX-U scenarios [108]. This hybrid MPC incorporates the discrete-time dynamics of NBI actuators as additional constraints. Through nonlinear simulations, it has been demonstrated that this hybrid MPC significantly improves control performance by reducing or eliminating oscillatory behavior in stored energy and damping oscillations in the safety factor profile.

Complementing these control advances, the development of real-time protection systems is crucial for enhancing operational safety and reliability. The NSTX-U Shorted Turn Protection (STP) system serves as a vital safety feature by employing a Kalman filter-based algorithm to monitor coil currents and detect faults, such as shorted turns in poloidal field coils, in real-time [109]. Upon detection of an anomaly, the system is designed to swiftly terminate the tokamak pulse to prevent damage. This system has undergone extensive validation using historical NSTX-U data in real-time simulations, proving its ability to detect various shorted turn scenarios reliably. A key advantage of the STP system is its independent operation from the main PCS, which contributes to enhanced safety, reliability, and isolation from other control

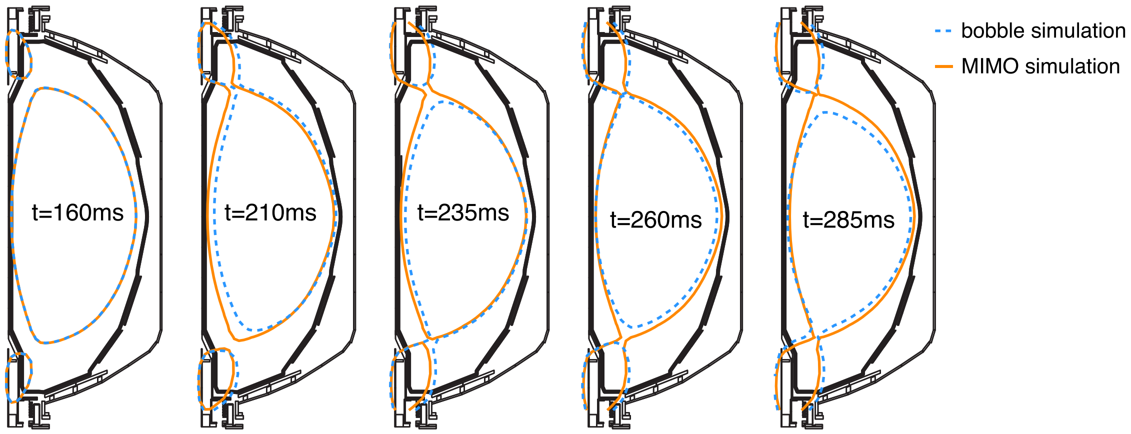

Figure 12. Time evolution of the plasma shape at different time instants for the bobble simulation (dashed blue) and simulation under MIMO control (solid orange). Reprinted from [105], Copyright (2025), with permission from Elsevier.

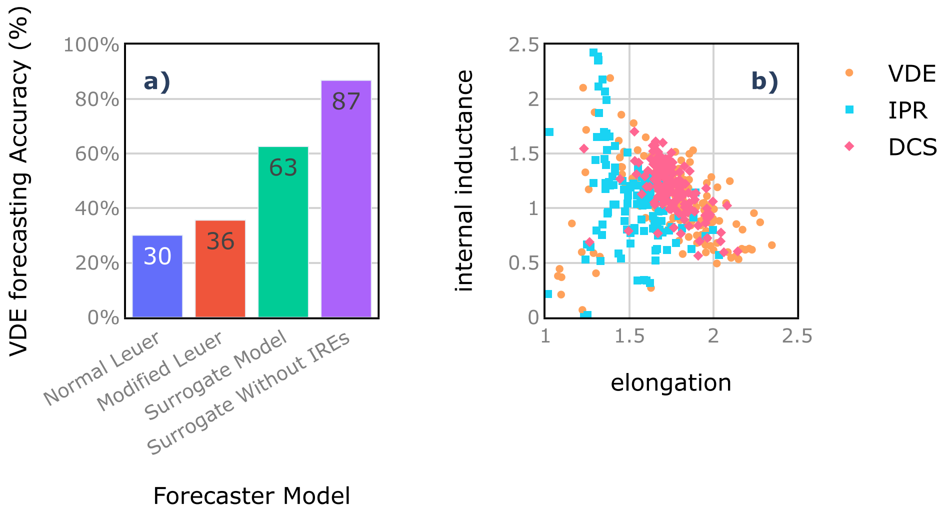

Figure 13. In (*a*), comparison of VDE forecasting accuracy for different methods of computing the Leuer stability criterion. Reproduced from [113]. © The Author(s). Published by IOP Publishing Ltd. CC BY 4.0. In (*b*), elongation and *li* values at the time of several NSTX-U disruptions. Reproduced from [111]. © 2024 The Author(s). Published by IOP Publishing Ltd on behalf of the IAEA. CC BY 4.0.

tasks, thereby allowing for quick implementation and deployment of various models during NSTX-U commissioning and upgrades.

4.3. Disruption prediction and avoidance

Disruptions, characterized by rapid loss of plasma confinement, pose a significant threat to future fusion power plants due to potential damage and downtime. Developing methods to predict and avoid these events is therefore crucial for the viability and longevity of fusion power plants.

By leveraging the DECAF [110] code's multi-device and multi-year analysis capabilities, the possibility to detect and avoid disruptions has been advanced. The disruption detection is enhanced through the identification of abnormal variations in plasma current (I_p) and vertical position (Z), such as I_p quenches, transient 'spikes', and vertical displacements [111]. Triggers of disruptive event chains consisting of these abnormalities were shown to occupy predominantly distinct regions of the operation space diagrams (see figure 13(*b*)). The implementation of an I_p quench-based binary classifier was highlighted as a robust and universal indicator of disruptive plasmas due to its general irreversibility and reliance on basic I_p measurements. Further understanding of causal disruptive event evolution is provided through DECAF's new capability distinguishing between naturally occurring disruptions from those caused by technical failures (such as hardware or software faults, PCS phase changes, etc). Particular focus was then posed in advancing the capability to forecast Vertical Displacement Events (VDEs). The possibility to use the Leuer criterion [112], a physics-based vertical stability metric, as an early warning forecaster was investigated [113]. To enable its real-time application, a linear surrogate model for the plasma current density profile was developed, allowing the profile to be reconstructed at a high time resolution (1.6 kHz), thereby enabling the potential real-time employment of the Leuer criterion. The achieved VDE forecasting accuracy is shown in figure 13(*a*). Further work is ongoing to couple it with other stability metrics for a more comprehensive and reliable VDE forecaster.

To identify the underlying conditions that lead to long-lasting improved confinement with RMS, a database was formed from NSTX data to study RMS using machine learning [114]. RMS discharges are prone to suffer from MHD events, which can cause current redistribution and often precede disruptions, resulting in the collapse of q_0 onto q_{min}. A primary focus was on categorizing RMS discharges based on their duration and formation, using magnetic field pitch angle data. With machine learning, NSTX shots with RMS were characterized as belonging to three distinctive groups, namely weak, strong and recovered RMS shots, helping to understand the plasma conditions that are susceptible to disruption-prone MHD events.

5. Conclusions

With the recovery project of NSTX-U now being more than 90% completed, its operation is planned to restart in the second half of 2026. In the meantime research on NSTX and NSTX-U has advanced using previous data from NSTX and NSTX-U as well comparing the results with other national and international devices. When NSTX-U restarts operation, it will represent a crucial step toward closing the physics gaps that will inform the realization of compact, cost-effective fusion pilot plants.

Data availability statement

The data that supports the findings of this study are openly available at [115].

Acknowledgment

This work was supported by the U.S. Department of Energy under contract numbers DE-AC02-09CH11466, DE-AC05-00OR22725, DE-AC52-07NA27344, DE-FG02-91ER54109, DE-FG02-95ER54309, DE-SC0008309, DE-SC0013977, DE-SC0021113, DE-SC0021120, DE-SC0021150, DE-SC0021271, DE-SC0021311, DE-SC0021385, DE-SC0021625, DE-SC0022051, DE-SC0022115 and DE-SC0022272. The United States Government retains a non-exclusive, paid-up, irrevocable, world-wide license to publish or reproduce the published form of this manuscript, or allow others to do so, for United States Government purposes.

ORCID iDs

S. Munaretto 0000-0003-1465-0971
P.O. Adebayo-Ige 0000-0003-0259-1433
H. Anand 0000-0002-9632-5680
G. Avdeeva 0000-0001-7072-7967
S.G. Baek 0000-0001-8029-3525
K. Barada 0000-0001-7724-8491
E. Belli 0000-0001-7947-2841
E.V. Belova 0000-0002-1525-1027
J.W. Berkery 0000-0002-8062-3210
T.N. Bernard 0000-0002-7331-9704
N. Bertelli 0000-0002-9326-7585
P. Bonofiglo 0000-0001-5057-7383
P.T. Bonoli 0000-0002-1620-9680
M.D. Boyer 0000-0002-6845-9155
J. Candy 0000-0003-3884-6485
C.S. Chang 0000-0002-3346-5731
H. Chung 0009-0008-0394-3377
C. Clauser 0000-0002-2597-5061
D. Corona 0000-0002-1291-1552
N.A. Crocker 0000-0003-2379-5814
R. De Levante Rodriguez 0000-0003-2681-3096
A. Diallo 0000-0002-0706-060X
J. Dominski 0000-0001-9380-2544
V.N. Duarte 0000-0001-8096-7518
F. Ebrahimi 0000-0003-3109-5367
E.D. Emdee 0000-0003-3334-2077
S. Ethier 0000-0002-2666-8733
N.M. Ferraro 0000-0002-6348-7827
E.L. Foley 0009-0003-1752-8397
E.D. Fredrickson 0000-0002-2439-4089
M.E. Galante 0009-0000-9814-9425
K.F. Gan 0000-0002-7207-3802
S. Gerhardt 0000-0002-2546-2194
R.J. Goldston 0000-0002-0368-5514
M. Gorelenkova 0000-0001-8487-1396
W. Guttenfelder 0000-0001-8181-058X
R. Hager 0000-0002-4624-3150
F.D. Halpern 0000-0002-0387-6038
J. Halpern 0000-0001-9370-8160
D. Hatch 0000-0002-1625-4385
F. Hoffmann 0000-0002-0927-1371
M.S. Islam 0000-0003-2019-4001
S.C. Jardin 0000-0001-6390-6908
S.M. Kaye 0000-0002-2514-1163
A. Khodak 0000-0002-8273-6614
J.E. Kinsey 0000-0001-9334-7473
A. Kleiner 0000-0002-5800-8027
E. Kolemen 0000-0003-4212-3247
S. Ku 0000-0002-9964-1208
M. Lampert 0000-0002-8462-8799
B. Leard 0000-0003-4141-080X
B.P. LeBlanc 0000-0003-1455-0129
J.B. Lestz 0000-0002-6975-1537
F.M. Levinton 0009-0001-2284-7881
P.-Y. Li 0000-0002-9525-4171
N.C. Logan 0000-0002-3268-7359
N.A. Lopez 0000-0001-5566-3731
R. Lunsford 0000-0003-3588-6801
T. Macwan 0000-0002-9767-0830
R. Maingi 0000-0003-1238-8121
J. McClenaghan 0000-0003-4735-0991
A.G. McLean 0000-0002-0697-4397
J.E. Menard 0000-0003-1292-3286
Y.-S. Na 0000-0001-7270-3846
A.O. Nelson 0000-0002-9612-1936

M. Ono 0000-0001-9849-9417
A. Pajares 0000-0001-9251-9675
A. Pankin 0000-0002-1406-2902
J. Parisi 0000-0003-1328-7154
F.I. Parra 0000-0001-9621-7404
M.S. Parsons 0000-0002-2428-3215
B.S. Patel 0000-0003-0121-1187
M. Podestá 0000-0003-4975-0585
F.M. Poli 0000-0003-3959-4371
M. Porcelli 0009-0007-6088-3422
T. Rafiq 0000-0002-2164-1582
R. Raman 0000-0002-2027-3271
J.D. Riquezes 0000-0003-2661-5110
S.A. Sabbagh 0000-0003-1077-8118
A. Sanchez-Villar 0000-0003-3727-9319
E. Schuster 0000-0001-7703-6771
S. Shiraiwa 0000-0001-5249-0441
T. Singh 0000-0003-0860-3626
S.P. Smith 0000-0003-1526-380X
D. Smith 0000-0003-0972-3638
V.A. Soukhanovskii 0000-0001-5519-0145
G.M. Staebler 0000-0002-1944-1733
B. Stratton 0000-0001-8830-3003
K.E. Thome 0000-0002-4801-3922
M. Tobin 0000-0003-2276-6448
I.U. Uzun-Kaymak 0000-0002-7625-1493
B. Van Compernolle 0000-0002-5853-6233
W.X. Wang 0000-0001-9415-1560
A.S. Welander 0009-0005-5063-7047
B.D. Wirth 0000-0002-0395-0285
J. Yang 0000-0001-8422-8464
V. Zamkovska 0000-0001-8437-4576
X. Zhang 0000-0003-3775-5821

References

[1] Peng Y.-K.M. and Strickler D.J. 1986 Features of spherical torus plasmas *Nucl. Fusion* **26** 769
[2] Peng Y.-K.M. 2000 The physics of spherical torus plasmas *Phys. Plasmas* **7** 1681–92
[3] Ono M. and Kaita R. 2015 Recent progress on spherical torus research *Phys. Plasmas* **22** 040501
[4] Brown T.G. *et al* 2026 The spherical tokamak advanced reactor (STAR) fusion power plant design *Fusion Eng. Des.* **222** 115461
[5] Chapman I.T., Cowley S.C. and Wilson H.R. 2024 The spherical tokamak for energy production: theme issue introduction *Phil. Trans. R. Soc. A* **382** 20230416
[6] Kingham D. and Gryaznevich M. 2024 The spherical tokamak path to fusion power: opportunities and challenges for development via public-private partnerships *Phys. Plasmas* **31** 042507
[7] Menard J.E. *et al* 2017 Overview of NSTX Upgrade initial results and modelling highlights *Nucl. Fusion* **57** 102006
[8] Berkery J.W. and Harrison J.R. 2025 A review of collaborative studies between the NSTX/-U and MAST/-U spherical tokamaks *Plasma Phys. Control. Fusion* **67** 053001
[9] McNamara S.A.M., Kaye S.M., Unterberg E.A., Asunta O. and Berkery J.W. 2025 The ST40 collaboration: a groundbreaking, first-of-its-kind, public-private partnership in fusion *Fusion Sci. Technol.* **0** 1–14
[10] Harrison J.R. *et al* 2024 Overview of physics results from MAST upgrade towards core-pedestal-exhaust integration *Nucl. Fusion* **64** 112017
[11] McNamara S.A.M. *et al* 2024 Overview of recent results from the st40 compact high-field spherical tokamak *Nucl. Fusion* **64** 112020
[12] Kurskiev G.S. *et al* 2024 Confinement, heating and current drive study in globus-m2 toward a future step of spherical tokamak program in ioffe institute *Phys. Plasmas* **31** 062511
[13] Ono M. *et al* 2000 Exploration of spherical torus physics in the NSTX device *Nucl. Fusion* **40** 557
[14] Costley A.E. and McNamara S.A.M. 2021 Fusion performance of spherical and conventional tokamaks: implications for compact pilot plants and reactors *Plasma Phys. Control. Fusion* **63** 035005
[15] Berkery J.W. *et al* 2024 NSTX-U research advancing the physics of spherical tokamaks *Nucl. Fusion* **64** 112004
[16] Jardin S.C., Ferraro N., Luo X., Chen J., Breslau J., Jansen K.E. and Shephard M.S. 2008 The M3D-C1 approach to simulating 3D 2-fluid magnetohydrodynamics in magnetic fusion experiments *J. Phys.: Conf. Ser.* **125** 012044
[17] Jardin S.C., Munaretto S., Ferraro N.M., Kaye S.M., Kleiner A. and Lyons B.C. 2024 MHD stability of spherical tokamak equilibria with non-monotonic q-profiles *Phys. Plasmas* **31** 0191934
[18] Jardin S.C. 2025 On resistive interchange, double tearing and resonant and non-resonant infernal modes in spherical tokamak negative central shear discharges *Phys. Plasmas* **32** 082503
[19] Manickam J., Pomphrey N. and Todd A.M.M. 1987 Ideal MHD stability properties of pressure driven modes in low shear tokamaks *Nucl. Fusion* **27** 1461
[20] Charlton L.A., Hastie R.J. and Hender T.C. 1989 Resistive “infernal” modes *Phys. Fluids B* **1** 798–803
[21] Jardin S.C., Ferraro N.M., Guttenfelder W., Kaye S.M. and Munaretto S. 2022 Ideal MHD Limited Electron Temperature in Spherical Tokamaks *Phys. Rev. Lett.* **128** 245001
[22] Munaretto S., Ferraro N.M. and Fredrickson E.D. 2023 On the frequency bifurcations of the MHD startup modes in NSTX *Phys. Plasmas* **30** 062502
[23] Jardin S.C., Ferraro N.M., Guttenfelder W., Kaye S.M. and Munaretto S. 2023 Ideal MHD induced temperature flattening in spherical tokamaks *Phys. Plasmas* **30** 042507
[24] Stutman D., Delgado-Aparicio L., Gorelenkov N., Finkenthal M., Fredrickson E., Kaye S., Mazzucato E. and Tritz K. 2009 Correlation between electron transport and shear Alfvén activity in the national spherical torus experiment *Phys. Rev. Lett.* **102** 115002
[25] Belova E.V., Fredrickson E.D. and Crocker N.A. 2024 Nonlinear simulations of GAEs in NSTX-U *Phys. Plasmas* **31** 0222439
[26] Candy J., Belli E.A. and Bravenec R.V. 2016 A high-accuracy Eulerian gyrokinetic solver for collisional plasmas *J. Comput. Phys.* **324** 73–93
[27] Gerhardt S.P. *et al* 2011 Recent progress towards an advanced spherical torus operating point in NSTX *Nucl. Fusion* **51** 073031
[28] McClenaghan J., Neiser T.F., Halpern F.D., Thome K.E., Turnbull A.D., DeShazer E.W., Meneghini O.M., Avdeeva G., Lestz J.B. and Candy J. 2025 Role of perturbed parallel magnetic field effects in predicting turbulent transport in NSTX *Plasma Phys. Control. Fusion* **67** 055013
[29] Candy J., Holland C., Waltz R.E., Fahey M.R. and Belli E. 2009 Tokamak profile prediction using direct gyrokinetic and neoclassical simulation *Phys. Plasmas* **16** 060704

[30] Singh T., Rafiq T., Schuster E., Lin Z. and Kuley A. 2025 Global gyrokinetic simulations of kinetic ballooning mode in NSTX-U plasmas *Nucl. Fusion* **65** 106039
[31] Patel B.S., Hardman M.R., Kennedy D., Giacomin M., Dickinson D. and Roach C.M. 2025 The impact of E × B shear on microtearing based transport in spherical tokamaks *Nucl. Fusion* **65** 026063
[32] Snyder P.B., Groebner R.J., Hughes J.W., Osborne T.H., Beurskens M., Leonard A.W., Wilson H.R. and Xu X.Q. 2011 A first-principles predictive model of the pedestal height and width: development, testing and ITER optimization with the EPED model *Nucl. Fusion* **51** 103016
[33] Diallo A. *et al* 2013 Progress in characterization of the pedestal stability and turbulence during the edge-localized-mode cycle on National Spherical Torus Experiment *Nucl. Fusion* **53** 093026
[34] Kleiner A., Ferraro N.M., Diallo A. and Canal G.P. 2021 Importance of resistivity on edge-localized mode onset in spherical tokamaks *Nucl. Fusion* **61** 064002
[35] Parisi J.F. *et al* 2024 Kinetic-ballooning-bifurcation in tokamak pedestals across shaping and aspect-ratio *Phys. Plasmas* **31** 0190818
[36] Parisi J.F. *et al* 2024 Kinetic-ballooning-limited pedestals in spherical tokamak plasmas *Nucl. Fusion* **64** 054002
[37] Parisi J.F. *et al* 2024 Stability and transport of gyrokinetic critical pedestals *Nucl. Fusion* **64** 086034
[38] Snyder P.B. *et al* 2009 Pedestal stability comparison and ITER pedestal prediction *Nucl. Fusion* **49** 085035
[39] Pankin A., Ebrahimi F., King J., Kleiner A. and Dominguez-Palacios J. 2025 Effects beyond ideal MHD on stability of wide and enhanced pedestal regimes in NSTX *Plasma Phys. Control. Fusion* **67** 095023
[40] Kleiner A., Imada K., Ebrahimi F., Ferraro N.M., Haskey S.R., Kogan L. and Pankin A. 2025 A study of resistive peeling-ballooning modes across spherical tokamaks *Plasma Phys. Control. Fusion* **67** 085026
[41] Jenko F. 2000 Massively parallel Vlasov simulation of electromagnetic drift-wave turbulence *Comput. Phys. Commun.* **125** 196–209
[42] Li P.-Y., Hatch D.R., Parisi J.F., Lampert M., Belli E.A., Kotschenreuther M. and Mahajan S.M. 2025 Importance of $\delta B_{\parallel}$ on ETG stability, turbulence and transport in NSTX *Nucl. Fusion* **65** 106040
[43] Dominski J., Guttenfelder W., Hatch D., Goerler T., Jenko F., Munaretto S. and Kaye S. 2024 Global micro-tearing modes in the wide pedestal of an NSTX plasma *Phys. Plasmas* **31** 0200894
[44] Pankin A.Y., Breslau J., Gorelenkova M., Andre R., Grierson B., Sachdev J., Goliyad M. and Perumpilly G. 2025 TRANSP integrated modeling code for interpretive and predictive analysis of tokamak plasmas *Comput. Phys. Commun.* **312** 109611
[45] Rafiq T., Kritz A.H., Weiland J., Pankin A.Y. and Luo L. 2013 Physics basis of Multi-Mode anomalous transport module *Phys. Plasmas* **20** 032506
[46] Leard B., Wang Z., Morosohk S., Rafiq T. and Schuster E. 2024 Fast neural-network surrogate model of the updated multi-mode anomalous transport module for NSTX-U *IEEE Trans. Plasma Sci.* **52** 4126–32
[47] Rafiq T., Wilson C., Clauser C., Schuster E., Weiland J., Anderson J., Kaye S.M., Pankin A., LeBlanc B.P. and Bell R.E. 2024 Predictive modeling of NSTX discharges with the updated multi-mode anomalous transport module *Nucl. Fusion* **64** 076024
[48] Rafiq T., Wilson C., Luo L., Weiland J., Schuster E., Pankin A.Y., Guttenfelder W. and Kaye S. 2022 Electron temperature gradient driven transport model for tokamak plasmas *Phys. Plasmas* **29** 092503
[49] Pankin A., McCune D., Andre R., Bateman G. and Kritz A. 2004 The tokamak Monte Carlo fast ion module NUBEAM in the National Transport Code Collaboration library *Comput. Phys. Commun.* **159** 157–84
[50] Boyer M.D., Kaye S. and Erickson K. 2019 Real-time capable modeling of neutral beam injection on NSTX-U using neural networks *Nucl. Fusion* **59** 056008
[51] Leard B., Rafiq T., Ward I., Galfrascoli F., Schuster E., Pankin A. and Gorelenkova M. 2025 Self-consistent equilibrium and transport simulations for NSTX-U plasmas enhanced via machine learning surrogate models *Fusion Eng. Des.* **219** 115201
[52] Chung H., Lee C.Y., Choi G.J., Kaye S.M., LeBlanc B.P., Berkery J.W. and Na Y.-S. 2025 Development of a data-driven neural network model for electron thermal transport in NSTX *Nucl. Fusion* **65** 086028
[53] Lee C.Y. *et al* 2021 Development of integrated suite of codes and its validation on KSTAR *Nucl. Fusion* **61** 096020
[54] Sánchez-Villar A.., Bai Z., Bertelli N., Bethel E.W., Hillairet J., Perciano T., Shiraiwa S., Wallace G.M. and Wright J.C. 2024 Real-time capable modeling of ICRF heating on NSTX and WEST via machine learning approaches *Nucl. Fusion* **64** 096039
[55] Sanchez-Villar A., Bai Z., Bertelli N., Bethel E.W., Hillairet J., Perciano T., Shiraiwa S., Wallace G.M. and Wright J.C. 2025 Machine learning enhanced predictions of ICRF heating: overcoming numerical limitations via data curation *Phys. Plasmas* **32** 0268341
[56] Sanchez-Villar A. *et al* 2026 Automated ICRF heating surrogate modeling via machine learning *EPJ Web Conf.* **346** 01005
[57] Brambilla M. 1999 Numerical simulation of ion cyclotron waves in tokamak plasmas *Plasma Phys. Control. Fusion* **41** 1
[58] Staebler G.M., Kinsey J.E. and Waltz R.E. 2005 Gyro-Landau fluid equations for trapped and passing particles *Phys. Plasmas* **12** 102508
[59] Staebler G.M., Belli E.A. and Candy J. 2023 A flexible gyro-fluid system of equations *Phys. Plasmas* **30** 102501
[60] Kinsey J.E., Staebler G.M., Belli E.A. and Candy J. 2025 Analysis of the impact of parallel magnetic fluctuations on linear gyrokinetic stability in NSTX-U and verification of gyro-fluid models *Phys. Plasmas* **32** 072301
[61] Clauser C.F., Rafiq T., Parisi J., Avdeeva G., Guttenfelder W., Schuster E. and Wilson C. 2025 Electron temperature gradient instability and transport analysis in NSTX and NSTX-U plasmas *Phys. Plasmas* **32** 0232697
[62] Lestz J.B., Avdeeva G., Kaye S.M., Gorelenkova M., Halpern F., McClenaghan J., Pankin A. and Thome K.E. 2025 Sensitivities of time-dependent temperature profile predictions for NSTX with the Multi-Mode Model *Plasma Phys. Control. Fusion* **67** 105030
[63] Lestz J.B., Avdeeva G., Neiser T., Gorelenkova M., Halpern F., Kaye S.M., McClenaghan J., Pankin A. and Thome K.E. 2025 Assessing time-dependent temperature profile predictions using reduced transport models for high performing NSTX plasmas *Plasma Phys. Control. Fusion* **67** 105029
[64] Lestz J., Avdeeva G., Neiser T., Gorelenkova M., Halpern F., Kaye S., McClenaghan J., Pankin A. and Thome K. 2025 Data for "Assessing time-dependent temperature profile predictions using reduced transport models for high performing NSTX plasmas" [Data set] Version 1 Princeton University (https://doi.org/10.34770/4dky-hh94)
[65] Avdeeva G., Thome K.E., Berkery J.W., Kaye S.M., McClenaghan J., Meneghini O., Odstrcil T., Sabbagh S.A., Smith S.P. and Turnbull A.D. 2024 Accuracy of kinetic equilibrium reconstruction of NSTX and NSTX-U

plasmas and its impact on the transport and stability analysis *Plasma Phys. Control. Fusion* **66** 115003

[66] Rognlien T.D., Milovich J.L., Rensink M.E. and Porter G.D. 1992 A fully implicit, time dependent 2-D fluid code for modeling tokamak edge plasmas *J. Nucl. Mater.* **196–198** 347–51

[67] Islam M.S., Umansky M.V. and Soukhanovskii V.A. 2025 Self-consistent modeling of tokamak edge plasma transport with lithium sources *Phys. Plasmas* **32** 092502

[68] Khodak A., Emdee E.D., Goldston R.J. and Maingi R. 2024 Design and analysis of liquid lithium plasma facing components *IEEE Trans. Plasma Sci.* **52** 4133–9

[69] Khodak A., Emdee E., Goldston R. and Maingi R. 2024 Coupled model for liquid lithium plasma facing components *Fusion Eng. Des.* **207** 114651

[70] Khodak A., Emdee E., Goldston R. and Maingi R. 2024 Liquid lithium divertor analysis using coupled plasma material interaction model *Nucl. Mater. Energy* **41** 101821

[71] Wiesen S. *et al* 2015 The new SOLPS-ITER code package *J. Nucl. Mater.* **463** 480–4

[72] Emdee E.D., Goldston R.J., Khodak A. and Maingi R. 2024 Optimization of lithium vapor box divertor evaporator location on NSTX-U using SOLPS-ITER *Nucl. Fusion* **64** 086047

[73] Emdee E.D. and Goldston R.J. 2024 Lithium vapor cave design considerations *Nucl. Mater. Energy* **41** 101737

[74] Parsons M.S., Porcelli M., Emdee E.D. and Goldston R.J. 2025 Thermal response of a lithium vapor divertor to cyclical operation *J. Fusion Energy* **44** 11

[75] Zweben S.J., Stotler D.P., Scotti F. and Myra J.R. 2017 Two-dimensional turbulence cross-correlation functions in the edge of NSTX *Phys. Plasmas* **24** 102509

[76] Lampert M., Diallo A. and Myra J.R. 2025 Evolution of intermittent filaments in the scrape-off layer of NSTX *Phys. Plasmas* **32** 102507

[77] Krasheninnikov S.I., D'ippolito D.A. and Myra J.R. 2008 Recent theoretical progress in understanding coherent structures in edge and SOL turbulence *J. Plasma Phys.* **74** 679–717

[78] D'Ippolito D.A., Myra J.R. and Zweben S.J. 2011 Convective transport by intermittent blob-filaments: comparison of theory and experiment *Phys. Plasmas* **18** 060501

[79] Lampert M., Diallo A., Myra J.R. and Zweben S.J. 2022 Internal rotation of ELM filaments on NSTX *Phys. Plasmas* **29** 102502

[80] Bernard T.N., Halpern F.D., Francisquez M., Juno J., Mandell N.R., Hammett G.W., Hakim A., Humble E. and Mukherjee R. 2023 Effect of neutral interactions on parallel transport and blob dynamics in gyrokinetic scrape-off layer simulations *Phys. Plasmas* **30** 0160588

[81] Zhang X. *et al* 2025 Core-edge integrated predictive studies of ST40 and NSTX plasmas with the scrape-off layer box model *Phys. Plasmas* **32** 0251145

[82] Adebayo-Ige P.O., Gan K.F., Lasnier C.J., Maingi R. and Wirth B.D. 2024 Divertor heat load estimates on NSTX and DIII-D using new and open-source 2D inversion analysis code *Nucl. Fusion* **64** 096006

[83] Herrmann A., Junker W., Gunther K., Bosch S., Kaufmann M., Neuhauser J., Pautasso G., Richter T. and Schneider R. 1995 Energy flux to the ASDEX-Upgrade diverter plates determined by thermography and calorimetry *Plasma Phys. Control. Fusion* **37** 17

[84] Gan K.F., Ahn J.-W., Park J.-W., Maingi R., McLean A.G., Gray T.K., Gong X. and Zhang X.D. 2013 2D divertor heat flux distribution using a 3D heat conduction solver in National Spherical Torus Experiment *Rev. Sci. Instrum.* **84** 023505

[85] Soukhanovskii V.A. *et al* 2024 In search of X-point radiator regime features in NSTX and DIII-D discharges with the snowflake divertor *Nucl. Mater. Energy* **41** 101790

[86] Gan K.F. *et al* 2025 Observation of stationary filaments with resonant magnetic perturbations in NSTX *Nucl. Fusion* **65** 096004

[87] Meade D. the TFTR Group 1991 Recent TFTR results *Plasma Physics and Controlled Nuclear Fusion Research 1990. Proc. 13th Int. Conf., (Washington, DC, 1 October–6 October 1990)* (*Proc. Series* vol 1) (International Atomic Energy Agency) pp 9–24

[88] Galante M.E., Boyer M.D., Uzun-Kaymak I.U., Foley E.L., LeBlanc B.P. and Levinton F.M. 2025 Reversed magnetic shear scenario development in NSTX-U using TRANSP *Nucl. Fusion* **65** 026035

[89] Yang J., Podestá M., Fredrickson E.D., Liu C., Berkery J.W. and Poli F.M. 2023 The role of fast ions in spontaneous neoclassical tearing mode instabilities in NSTX *Plasma Phys. Control. Fusion* **65** 064004

[90] Liu C., Jardin S.C., Qin H., Xiao J., Ferraro N.M. and Breslau J. 2022 Hybrid simulation of energetic particles interacting with magnetohydrodynamics using a slow manifold algorithm and GPU acceleration *Comput. Phys. Commun.* **275** 108313

[91] Hirshman S.P. and Whitson J.C. 1983 Steepest-descent moment method for three-dimensional magnetohydrodynamic equilibria *Phys. Fluids* **26** 3553–68

[92] Halpern J., Logan N.C., Paul E. and Paz-Soldan C. 2025 Determining the validity of tokamak perturbed equilibrium modeling using nonlinear equilibria *Nucl. Fusion* **65** 106028

[93] Wang W.X., Yoo M.G., Startsev E.A., Kaye S., Ethier S. and Chen J. 2024 Plasma self-driven current in tokamaks with magnetic islands *Nucl. Fusion* **65** 016008

[94] Smirnov A.P., Harvey R.W. and Kupfer K. 1994 A general ray tracing code GENRAY *Bull Am. Phys. Soc* **39** 1626

[95] Petrov Y.V. and Harvey R.W. 2016 A fully-neoclassical finite-orbit-width version of the CQL3D Fokker-Planck code *Plasma Phys. Control. Fusion* **58** 115001

[96] Van Compernolle B., Jian X., Bertelli N., Desai S., Lestz J.B., McClenaghan J., Ono M., Pinsker R.I. and Thome K. 2025 Parametric raytracing modeling for NSTX-U scenario development with high harmonic fast waves and neutral beam injection *Plasma Phys. Control. Fusion* **67** 065018

[97] Taylor G. *et al* 2012 High non-inductive fraction H-mode discharges generated by high-harmonic fast wave heating and current drive in the National Spherical Torus Experiment *Phys. Plasmas* **19** 042501

[98] Hosea J. *et al* 2008 High harmonic fast wave heating efficiency enhancement and current drive at longer wavelength on the National Spherical Torus Experiment *Phys. Plasmas* **15** 056104

[99] Shiraiwa S., Wright J.C., Bonoli P.T., Kolev T. and Stowell M. 2017 RF wave simulation for cold edge plasmas using the MFEM library *EPJ Web Conf.* **157** 03048

[100] Rodriguez R.D.L., Baek S.-G., Shiraiwa S.'i.c.h.i., Bertelli N. and Bonoli P. 2025 Effects of midplane density gradient in the propagation of high-harmonic fast waves considering high temperature anisotropy in the scrape-off layer of NSTX-U *Phys. Scr.* **100** 105601

[101] Bertelli N., Shiraiwa S. and Ono M. 2022 3D full wave fast wave modeling with realistic HHFW antenna geometry and SOL plasma in NSTX-U *Nucl. Fusion* **62** 126046

[102] Kolemen E., Gates D.A., Gerhardt S., Kaita R., Kugel H., Mueller D., Rowley C. and Soukhanovskii V. 2011 Plasma modelling results and shape control improvements for NSTX *Nucl. Fusion* **51** 113024

[103] Parisi J.F. *et al* 2025 Doubling fusion power with volumetric optimization in magnetic confinement fusion devices *Phys. Rev. Res.* **7** 013139
[104] Welander A.S., Wehner W.P., Pajares A. and Thome K.E. 2024 Virtual Tokamak for test and development of plasma control applied to NSTX-U *IEEE Trans. Plasma Sci.* **52** 3898–903
[105] Pajares A., Welander A.S., Wehner W.P., Thome K.E., Eidietis N.W. and Anand H. 2025 Plasma shape and position control development for NSTX-U using the GSEvolve plasma simulator *Fusion Eng. Des.* **220** 115302
[106] Battaglia D.J. *et al* (the NSTX-U Research, Operations and Engineering Team) 2018 Scenario development during commissioning operations on the National Spherical Torus Experiment Upgrade *Nucl. Fusion* **58** 046010
[107] Boyer M.D. *et al* 2018 Plasma boundary shape control and real-time equilibrium reconstruction on NSTX-U *Nucl. Fusion* **58** 036016
[108] Leard B., Wang Z., Paruchuri S.T., Schuster E. and Rafiq T. 2024 Hybrid model predictive control techniques for safety factor profile and stored energy regulation while incorporating NBI constraints *Nucl. Fusion* **64** 086052
[109] Corona D., Boyer D., Comanescu M., Hoffmann F. and Gerhardt S. 2025 Enhancing operational safety: the NSTX-U Shorted Turn Protection (STP) system *Fusion Eng. Des.* **213** 114784
[110] Sabbagh S.A. *et al* 2023 Disruption event characterization and forecasting in tokamaks *Phys. Plasmas* **30** 032506
[111] Zamkovska V. *et al* 2024 DECAF cross-device characterization of tokamak disruptions indicated by abnormalities in plasma vertical position and current *Nucl. Fusion* **64** 066030
[112] Leuer J.A. 1989 Passive vertical stability in the next generation tokamaks *Fusion Technol.* **15** 489–94
[113] Tobin M. *et al* 2024 Vertical instability forecasting and controllability assessment of multi-device tokamak plasmas in DECAF with data-driven optimization *Plasma Phys. Control. Fusion* **66** 105020
[114] Uzun-Kaymak I.U., Foley E.L., Galante M.E. and Levinton F.M. 2024 Forming a database to study reversed magnetic shear from the National Spherical Torus eXperiment using machine learning *Phys. Plasmas* **31** 0222490
[115] Munaretto S. *et al* 2025 Data for “Spherical tokamak physics research in preparation for the operation of NSTX-U” [Data set] Version 1 Princeton Plasma Physics Laboratory, Princeton University (https://doi.org/10.34770/m33t-7777)